METAL DICYANAMIDES AS SOLID ADSORBENTS FOR CO_2/N_2 SEPARATION AND EFFICIENT WATER OXIDATION CATALYSTS

A THESIS SUBMITTED TO

THE GRADUATE SCHOOL OF ENGINEERING AND SCIENCE

OF BILKENT UNIVERSITY

IN PARTIAL FULFILLMENT OF THE REQUIREMENTS FOR

THE DEGREE OF

MASTER OF SCIENCE

IN

CHEMISTRY

By

Aysun Başaran

July 2016

METAL DICYANAMIDES AS SOLID ADSORBENTS FOR CO_2/N_2 SEPARATION AND EFFICIENT WATER OXIDATION CATALYSTS

By Aysun Başaran

July 2016

We certify that we have read this thesis and that in our opinion it is fully adequate,

in scope and in quality, as a thesis for the degree of Master of Science.

_____

Ferdi KARADAŞ (Advisor)

_____

Ömer DAĞ

_____

Atilla CİHANER

Approved for the Graduate School of Engineering and Science:

_____

Levent ONURAL

Director of the Graduate School

ABSTRACT

METAL DICYANAMIDES AS SOLID ADSORBENTS FOR CO_2/N_2 SEPARATION AND EFFICIENT WATER OXIDATION CATALYSTS

Aysun Başaran

M.S. in Chemistry

Advisor: Ferdi KARADAŞ

July 2016

The demand for the energy has been increasing exponentially and it is expected to double by 2050 as a result of population increase in the world. The fact that fossil-based fuels are limited and they releases CO_2 gas, which affects the environment negatively. This situation encourages researchers to two important disciplines of science: 1) removal of CO_2 from atmosphere and 2) developing alternative sources of energy that are clean and efficient.

Low carbon future will be realized by post-combustion CO_2 capture with air separation therefore adsorbents are needed for CO_2 capture. Since surface volume, adsorption enthalpy, and functional groups inside the pores affect the interactions between CO_2 and surface, new porous materials should be designed specifically that possess all of the aforementioned features. In this thesis study, a new metal dicyanamide compound, $Co(hmt)(dca)_2$, with free nitrogen atoms in the pores were synthesized. A high adsorption of CO_2 was observed while the material exhibits almost no N_2 uptake at room temperature. In the $Co(hmt)(dca)_2$ crystal, the pore opening defined as almost 3.8 Å and kinetic diameters of N_2 and CO_2 are 3.6 Å and 3.3 Å, respectively. There is a similarity between kinetic diameter of the crystal and N_2 resulting in limited diffusion of N_2 and it is the origin of the high selectivity obtained in this

study. Although metal dicyanamides have widely been studied in different fields it is the first study in the area of CO_2 gas storage.

The negative effects of the CO_2 level can also be overcome by developing alternative sources of energy that are carbon-free. Hydrogen economy, which involves splitting water using light to produces O_2 and H_2 has received much attention in the recent years since it is carbon-free and it is based on only water and sun light that are of great abundance. Novel catalysts should be developed to overcome one of the most challenging steps of hydrogen economy, water oxidation, which is one of the half reactions of water splitting. In this thesis study, simple metal dicyanamides have been investigated as water oxidation catalysts. A new family of metal dicyanamides with the formula, $M(dca)_2(DMF)_2$, (M = Co, Ni, and Fe), was synthesized and characterized. A current density of 1 $mA.cm^{-2}$ obtained at an overpotential of 580 mV and by Ni doping the value could be decreased down to 513 mV. This is the first study that involves the application of cobalt-dicyanamide systems in electrochemical water oxidation catalysis. Electrocatalytic studies as well as long term (70 h) electrolysis studies show that these materials can efficiently oxidize water and are robust during long courses catalytic processes.

***Keywords*:** Energy, gas storage, metal dicyanamides compounds, porous material, water oxidation catalyst

ÖZET

CO_2/N_2 GAZ KARIŞIMININ AYRILMASI İÇİN KATI ABSORBAN VE ETKİLİ SU OKSİTLEYİCİ KATALİZÖRLER OLARAK METAL DİSİYANAMİT BİLEŞİKLERİNİN KULLANILMASI

Aysun Başaran

Kimya, Yüksek Lisans

Tez Danışmanı: Ferdi KARADAŞ

Temmuz 2016

Enerjiye olan ihtiyaç katlanarak artmakta ve 2050 yılında nüfus artışından dolayı bu ihtiyacın ikiye katlanması beklenmektedir. Fosil kaynaklı yakıtlar kısıtlıdır ve çevreyi olumsuz etkileyen CO_2 gazı yayarlar. Bu durum araştırmacıları iki önemli disipline teşvik etmektedir: 1) atmosferden CO_2 uzaklaştrılması ve 2) temiz ve etkili alternatif enerji kaynaklarının geliştirilmesi.

Karbon emisyonunun azaltılması için endüstriyel işlem sonrası CO_2'i seçici olarak ayırabilecek katı adsorbanların geliştirilmesine ihtiyaç vardır. Yüzey alanı, adsorpsiyon entalpisi ve boşluklardaki fonksiyonel gruplar gibi etkenler CO_2 ve yüzey alanının etkileşimini etkilediği için bahsedilen bütün özelliklere sahip olan yeni gözenekli malzemeler tasarlanmalıdır. Bu tez çalışmasında, gözeneklerinde serbest azot atomu bulunduran yeni metal disiyanamit bileşiği $Co(hmt)(dca)_2$ sentezlenmiştir. Yüksek CO_2 tutunumu oda sıcaklığında gözlemlenmesine rağmen malzemede N_2 alımı sergilenmemiştir. $Co(hmt)(dca)_2$ bileşiğinde boşluklar arası 3.8 Å, N_2 ve CO_2 kinetik yarıçapları ise 3.6 Å and 3.3 Å olarak belirtildi. Kristal ve N_2 arasındaki kinetik yarıçap benzerliği N_2 difüzyonunu kısıtlayarak

seçiciliği arttırmaktadır.Metal disiyanamit bileşikleri farklı alanlarda yaygın olarak çalışılmasına rağmen CO_2 gaz depolama alanındaki ilk çalışmadır.

CO_2 oranının olumsuz etkileri, karbon içermeyen alternatif enerji kaynakları geliştirilerek aşılabilir. O_2 ve H_2 üretimi için suyun ışıkla ayrıştırılmasını içeren Hidrojen ekonomisinin, karbon içermeyen sadece su ve güneş ışığına dayanması son zamanlarda çok ilgi çekmiştir. Hidrojen ekonomisinin en zor basamağı olan yarı reaksiyonlardan suyun oksitlenmesi aşaması, özgün katalizörlerin geliştirilmesiye aşılabilir. Bu tez çalışmasında, basit metal disiyanamit bileşikleri su oksitleyici katalizör olarak incelenmistir. Yeni bir metal disiyanamit ailesi $M(dca)_2(DMF)$, (M = Co, Ni, Fe) sentezlenip, karakterize edilmiştir. 1 $mA.cm^{-2}$ akım yoğunluğu 580 mV aşırı potansiyelde elde edildi ve bileşiğe Ni ekleyerek aşırı potansiyel 513 mV'a kadar düşürüldü. Bu çalışma, kobalt disiyanamit bileşiklerinin elektrokimyasal su oksitleyici katalizör olarak kullanıldığı ilk çalışmadır. Elektrokatalik çalışmaları ve uzun süreli elektroliz calışmaları bu malzemelerin etkili bir biçimde suyu oksitlediğini ve uzun süreli katalitik işlem boyunca da dayanıklı olduğunu göstermektedir.

***Anahtar Sözcükler*:** Enerji, gaz depolama, metal disiyanamit bileşikleri, gözenekli malzeme, su oksitleyici katalizör

ACKNOWLEDGEMENT

It is a great pleasure to thank my supervisor Assist. Prof. Ferdi Karadaş for his patience, guidance and motivation. He always supported me throughout my thesis and shared his knowledge. I always feel so lucky for working such a great, helpful and understanding advisor.

I also would like to thank thesis committee members Prof. Dr. Ömer Dağ, and Prof. Dr. Atilla Cihaner for their suggestions and patient.

I would like to thank The Scientific and Technological Research Council of Turkey, TÜBİTAK, for supporting my study and accepting to the National Scholarship 2210-C Programme for MSc Students. Additionally, I also would like to thank The Scientific and Technological Research Council of Turkey- Defense Industries Research and Development Institute, TÜBİTAK-SAGE, for permission to complete my MSc thesis.

I offer so many thanks to our group members Dr. Emine Ülker and Dr. Satya Vijay Kumar Nune for their encouragement and sharing valuable experiences. I also thank to Pınar Alsaç, Dr. Rupali Mishra, Saghir Abbas and Merve Demirkıran for their enjoyable friendships and supports.

I want to express my special thanks to my family for their endless love and support. They always encouraged me throughout my life, life is better with you.

Finally, I would like to offer my endless thanks to my all, my husband: Caner BAŞARAN. The are no words to express my gratitude for all things you have done for me. Thank you with all my heart for your patience, support and love.

To My Family...

Contents

List of Figures

List of Tables

Abbreviation

Γ	: Surface coverage (surface concentration)
η	: Overpotential
υ	: Potential scan rate
BET	: Brunauer–Emmett–Teller
CV	: Cyclic voltammetry
DCA	: Dicyanamide
DMF	: Dimethylformamide
E	: Potential
E^o	: Standard redox potential
$E_{1/2}$	: Half-wave potential
EDX	: Electron Dispersive X-ray spectroscopy
F	: Faraday's constant
FTIR	: Fourier Transform Infrared Spectroscopy
FTO	: Fluorine doped Tin Oxide
HMT	: Hexamethylenetetramine
KPi	: Potassium phosphate buffer
PXRD	: Powder X-Ray Diffraction
SEM	: Scanning Electron Microscopy
TGA	: Thermogravimetric Analysis
TOF	: Turnover frequency
WOC	: Wateroxidation catalyst
XRD	: X-ray Diffraction
XPS	: X-ray Photoelectron Spectroscopy

Chapter 1

INTRODUCTION

1.1. The Dicyanamide Chemistry

In the past few years, coordination polymers have attracted great interest because of the potential applications in the fields of magnetism, gas sorption, and catalysis.[1–3] The ligand dicyanamide (dca), $[N(CN)_2]^-$, which was first utilized by Köhler[4–6], has been widely studied for many years to design polymeric structures since it serves as a convenient bridging group to connect metal ions using its N-donor atoms. It is frequently referred as a 'pseudohalide' due to its negative charge. The dicyanamide is a versatile ligand and compounds with various structures ranging from one-dimesional to three-dimensional networks with different properties can be obtained.[7–10] This variety is mainly due to the possibility of dicyanamide anion to bind metal ions in eight different ways. To illustrate the binding between metal ion and nitrogen atom in the dicyanamide anion, a notation $\mu_{a,b,c,d,e}$ is used, where subscripts define the position of nitrogen atom.[1] The possible coordination modes, monodentate, bidentate, tridentate, and tetradentate are illustrated in Figure 1. μ_1 and μ_3 are monodentate notation; μ_1 defines the binding to metal ion through one of the nitrile nitrogen atoms and μ_3 defines the binding to metal ion by amide N-atom. $\mu_{1,5}$ is bidentate and bind to metal ions by nitrile N atoms. $\mu_{1,3}$ is also bidentate and shows binding to metal ions through both nitrile and amide N atom. $\mu_{1,3,5}$ and $\mu_{1,1,5}$ are tridentate and at first both nitrile N atoms and amide N atom are used to bind metal ions, at last one of the nitrile N atoms binds to two different metal ions and other nitrile N atom binds to metal ion.

A tetradentate possible binding notation $\mu_{1,1,3,5}$ means one of the nitrile N atom and amide N atom are μ-coordinated and the other nitrile atom bis-bidentate to different metal ions.[6] The rare alternative for binding to metal ion, $\mu_{1,1,3,5,5}$ represents the two different metal ion bindings by both nitrile N atom and a central amide N atom binding to metal.

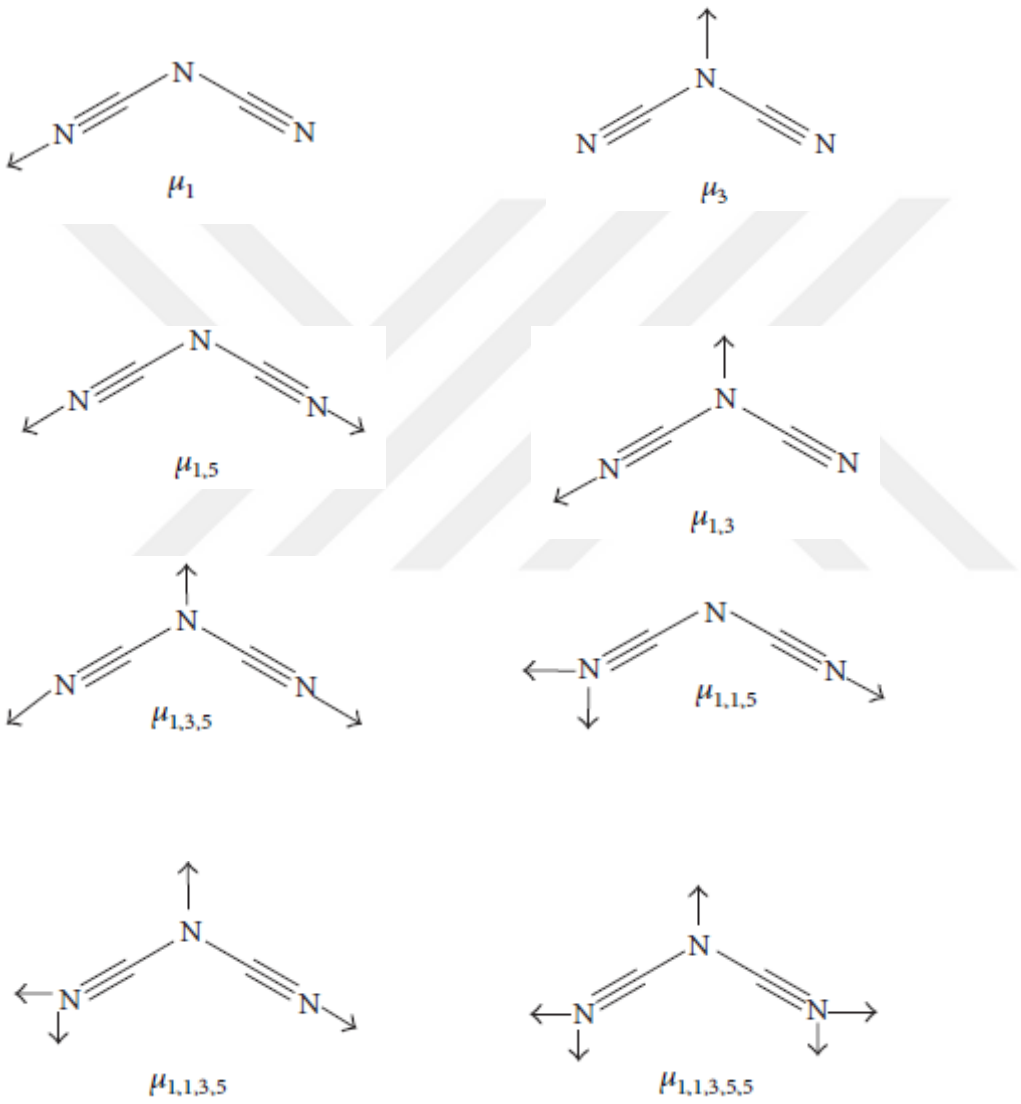

Figure 1. Possible dicyanamide coordination modes [11]

Coordination to metal through nitrile N atom is more possible compared to amide N atom coordination because of the high electron density on the terminal N-atoms.[12] Therefore, $\mu_{1,5}$ is the most common type of binding modes observed in dicyanamide-based compounds.

To determine coordination modes of dicyanamide anion, vibrational spectroscopy can be applied to monitor the shift in *ν*(CN). Typically, strong *ν*(CN) bands of free ions can be observed at 2232 cm^{-1} in addition to 2179 cm^{-1} for dicyanamide anion in the sodium salt.[12] If there is a monodentate coordination of dicyanamide anion by nitrile N atom as μ_1 two bands will be shown and the ranges of bands are generally 2235-2220 cm^{-1} and 2175-2160 cm^{-1}. The *ν*(CN) vibration will shift to higher frequencies when there is coordination through amide N-atom like μ_3. Bidentate coordination to metal ion $\mu_{1,3}$ and $\mu_{1,5}$ shows *ν*(CN) vibration almost 2250-2235 and 2200-2190 cm^{-1}. Vibration ranges, however, are not enough to distinguish the coordination modes of bidentate $\mu_{1,3}$ and $\mu_{1,5}$ binding modes. The *ν*(CN) vibration of tridentate coordination mode, $\mu_{1,3,5}$, could be observed within the ranges of 2280-2260 and 2220-2210 cm^{-1}. Although coordination mode does not have an influence on other vibration frequencies like ν_{as}(N-C) in dicyanamide anion, there is a characteristic strong band around 2280 cm^{-1} related to $\nu_s+\nu_{as}$(C-N) of dicyanamide compounds.[12]

Metal dicyanamide [$M(dca)_2$] compounds have been studied since the mid 1960s and mainly two phases were determined. One of the phases is α-[$M(dca)_2$], where M= Mn, Fe, Co, Ni, and Cu. The other phase is β-[$M(dca)_2$], where M= Mn, Co, and Zn. In the α phase, there are octahedral metal centers in addition to tridentate dca ligands. On the other hand, the β phase includes tetrahedral metal centers with bidentate dca ligands.

In 1998, Batten clearly reported the crystal structure of α-[M(dca)$_2$], which consists of a single rutile-like network as illustrated in Figure 2.[9,13]

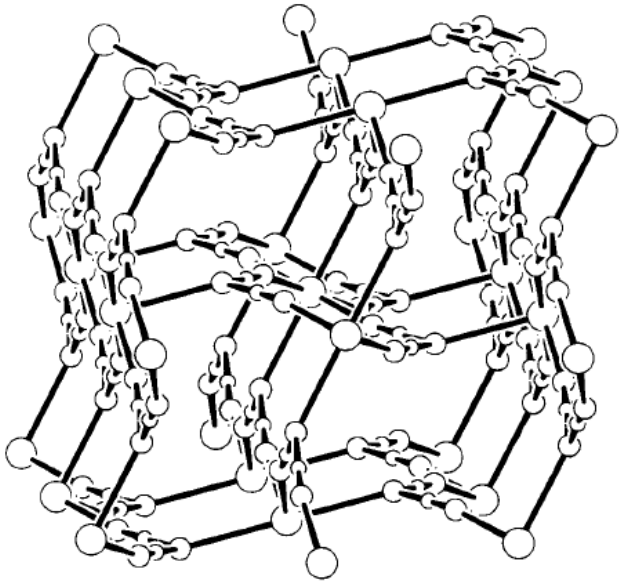

Figure 2. The rutile-related structure of Cu(dca)$_2$. The circles represent in order of decreasing size Cu, N and C.[9,13]

In the rutile-related structure of Cu(dca)$_2$, each dicyanamide anion is coordinated to three metal atoms through two nitrile and one amido central nitrogen. Coordination of each copper includes six dicyanamide ligands, four of which are nitrile nitrogens while the rest are amide nitrogens. Cu(II) site shows significant Jahn-Teller distortion with the two axial amide nitrogens noticeably further from the Cu(II) atom than the four equatorial nitrile nitrogens. Batten *et al.*[9] reported the presence of long-range ferromagnetic order exhibited by Co(dca)$_2$ and Ni(dca)$_2$ with *Tc* values of 9 and 20 K, respectively. Until recently, Cu(dca)$_2$ was thought to have no magnetic ordering due to Jahn-Teller distortion since elongation of axial Cu-N amide bonds leads to weaker Cu-Cu magnetic interactions. Recently, ferromagnetic ordering was detected below 1.7 K.[14]

The compound β-[Co(dca)$_2$] is isostructural to α-[Cu(dca)$_2$] and the structure is shown in Figure 3.[12]

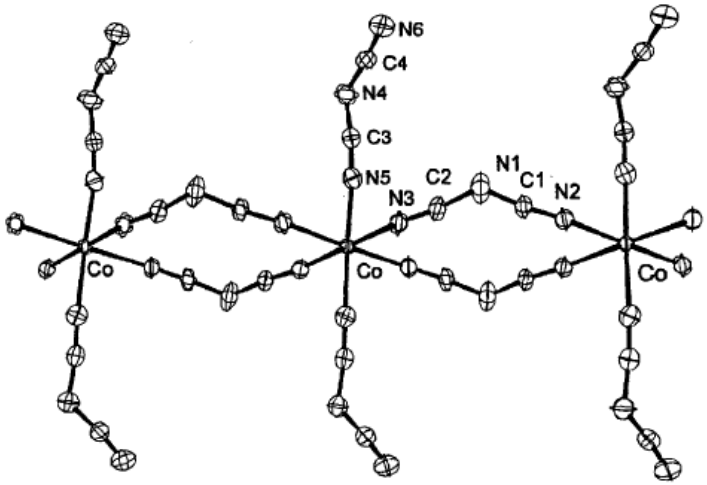

Figure 3. Structure of the sheet in β-[Co(dca)$_2$][12]

β-[Co(dca)$_2$] consists of metal atoms connected to the dicyanamide ligands only through nitrile nitrogens.

1.2. Modification of Metal-Dicyanamide Compounds

The topology of metal-dicyanamide network can be modified via the introduction of a coligand or cation templation. Coligands can be a variety of molecules and they can be classified as terminal and bridging ligands.[15] Given that dicyanamide ligand can also be coordinated to metal ion through various coordination modes as explained in the previous section, the concept of metal-dicyanamide coligand compounds is diverse covering many different structures and properties. In addition to this diversity, introducing coligand or cation templation make the metal dicyanamide compounds more open to crystal engineering of coordination polymers in the fields of gas adsorption and magnetism.[9]

1.2.1. Metal Dicyanamide Compounds with Terminal Coligands

Terminal non-bridging coligands are generally employed to occupy certain positions of metal coordination sphere. For example, when terminal coligand such as pyridyl group is incorporated into structure metal atoms are coordinated to pyridine nitrogen atoms and 1D chains can be obtained.[3] As a terminal coligand, pyridine, imidazole, 2-aminopyrimidine, 2,2'-bipyridine, 4-cyanopyridine,1,10–phenanthroline, 1,3-diaminopropane can be used (Figure 4), and they are widely used to modify metal dicyanamide compounds.

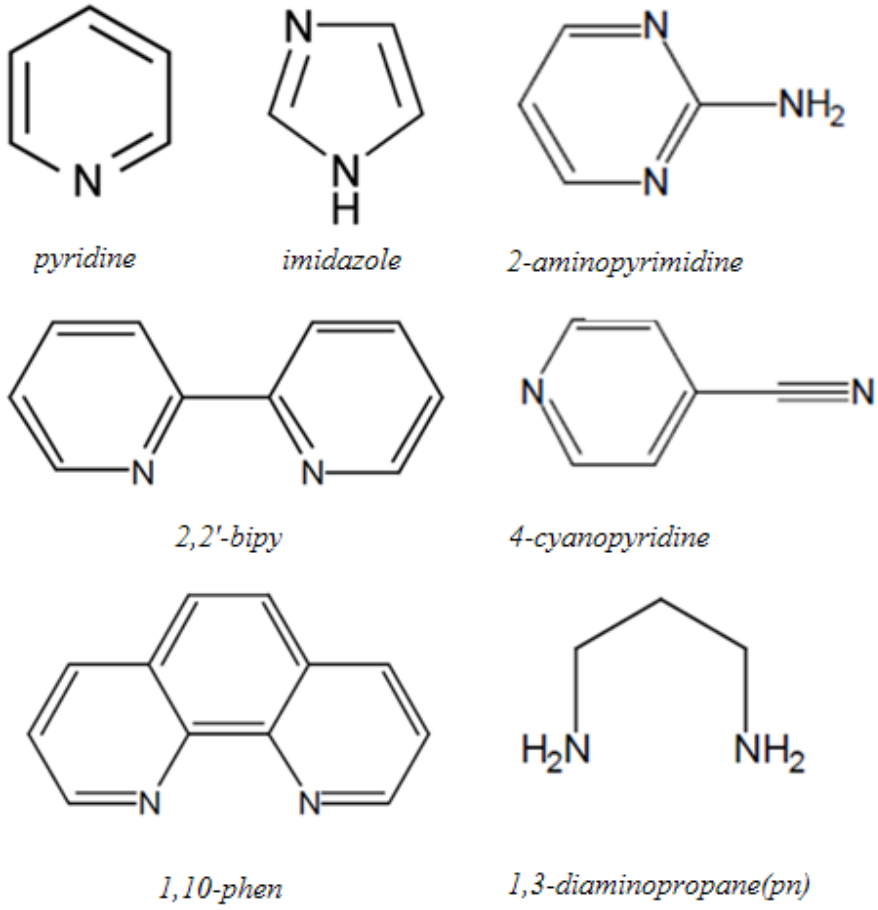

Figure 4. Possible Terminal Coligands

The simplest 1D network geometry can be a linear or zigzag shaped, in the structure just one bridging dicyanamide is connected to the per metal. Compared to only one dicyanamide per metal coordination, two bridging $\mu_{1,5}$–dca ligands per metal is more common. In Figure 5, $Mn(dca)_2(pyridine)_2$ with a linear structure is shown. In the structure, terminal pyridine ligands are in trans arrangement with a linear geometry.[10] The metal atoms next to each other are connected by two dicyanamide ligands and metal ions are linked to each other by four equatorial dca ligands into a linear chain.[10]

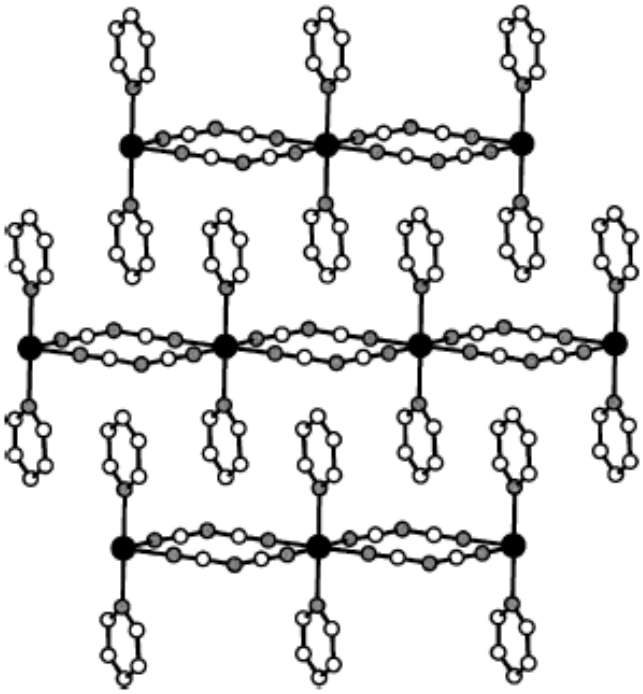

Figure 5. Linear chain structure of $Mn(dca)_2(pyridine)_2$[10,16,17]

The other form of 1D network is zigzag and it includes two bridging ligands per metal. The zigzag structure of $Cd(dca)_2$(2,2'-bipy) illustrated in Figure 6. In zigzag chain, terminal ligands are in cis arrangement.

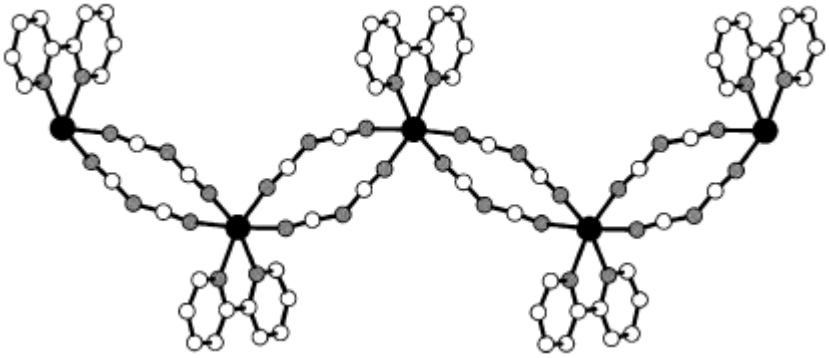

Figure 6. Zigzag chain structure of $Cd(dca)_2$(2,2'-bipy)[10,18]

The metal dicyanamide compounds with terminal or non-bridging coligand in 2D network are also examined. One of the most popular structure in 2D network is the $Mn(dca)_2$(4-cyanopyridine)$_2$.[10,19] In the compound coligands are in trans position as shown in Figure 7.

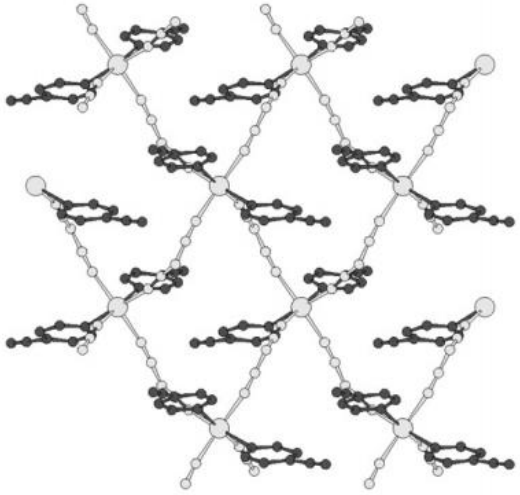

Figure 7. 2D structure of $Mn(dca)_2$(4-cyanopyridine)$_2$[10,19]

Another example for metal dicyanamide compounds with 2D framework is $Cd(dca)_2$(1,10-phen) as shown in Figure 8. [10,18]

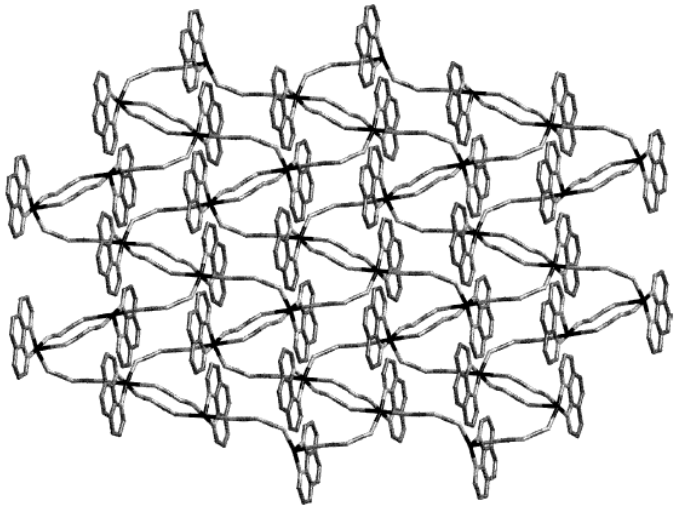

Figure 8. 2D structure of $Cd(dca)_2$(1,10-phen)

One of the examples of 3D metal dicyanamide networks with terminal coligand is $[Cu(pn)_2][Mn(dca)_4]$, pn=1,3-diaminopropane in Figure 9.[10,20]

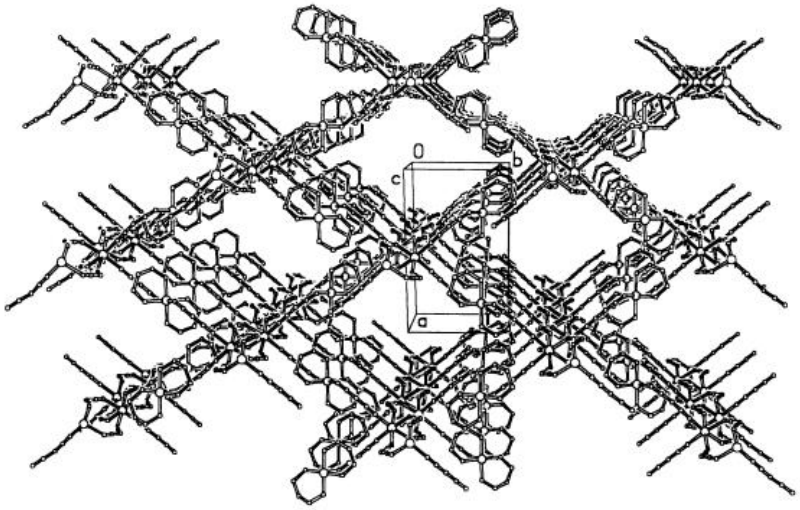

Figure 9. 3D structure of$[Cu(pn)_2][Mn(dca)_4]$

Overall, metal dicyanamide compounds can be modified with terminal coligands resulting in different topologies and dimensionalities. When metal atoms are coordinated to pyridine nitrogen atoms, 1D structure can be obtained. To extend the chain to 2D or 3D architectural network, π-π stacking interactions from pyridyl groups and hydrogen bonding interactions from uncoordinated groups and the intermolecular interactions are included in the extended network.[3]Although there is an exception, many compounds with a typical $\mu_{1,5}$-dicyanamide bridging show very weak antiferromagnetic coupling.

1.2.2. Metal Dicyanamide Compounds with Bridging Coligands

Bridging coligands are incorporated to metal dicyanamide compounds to increase dimensionality with coordination interaction. Pyrazine and 4,4'-bipyridine[21], illustrated in Figure 10, are widely used in metal dicyanamide compounds as bridging ligands. Dicyanamide act as a connector and bridge longer distances. To stabilize the network, hydrogen bond of structures will be accepted by uncoordinated nitrogen atoms.

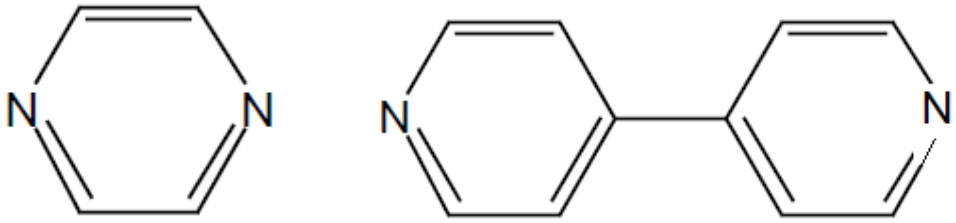

Pyrazine *4,4-bipy*

Figure 10. Possible Bridging Coligands

In the $Co(dca)_2$(pyrazine) structure, illustrated in Figure 11, metal centers are connected by double $\mu_{1,5}$-dca bridges and the linear chains are bridged to each other by pyrazine ligands.

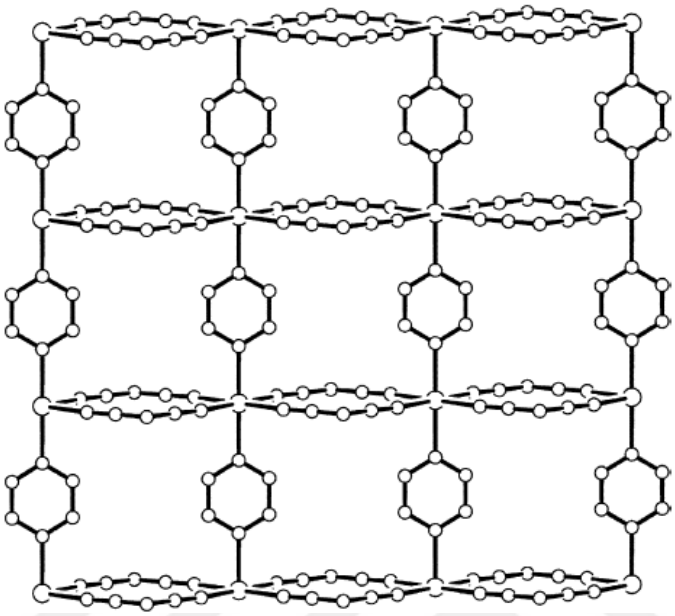

Figure 11. Structure of $Co(dca)_2$(pyrazine)[10]

Similar to pyrazine, 4,4'-bipyridine ligand is also a linear pyridyl-donor bridging ligand. 4,4'-bipyridine bridging coligand is longer in structure and so has the possibility to generate more different structures with metal dicyanamide compounds.

When dca ligands are modified with bridging coligand, a diverse range of 1D, 2D, and 3D structural networks can be obtained. Although there are exceptions, $\mu_{1,5}$-dca binding typically shows very weak antiferromagnetic coupling.

1.2.3. Anionic Metal Dicyanamide Compounds with Cation Templation

The topology of metal dicyanamide compounds can also be modified by creating anionic metal dicyanamide network. To create diverse anionic networks like $M(dca)_3^-$ and $M(dca)_4^-$ topologies, countercations like Ph_4E^+ and $R_4N^+$with different sizes, shapes, and charges are used in the netwok.

The $Mn(dca)_3^-$ network are modified by cation templation using Ph_4E (E=P, As) as shown in Figure 12. [10,22,23] In the structure, metal ions are connected to each other by single $\mu_{1,5}$-dca in one direction while metal ions are connected to each other by double $\mu_{1,5}$-dca bridges in the other direction creating $(Ph_4E)Mn(dca)_3$ with a 2D topology.

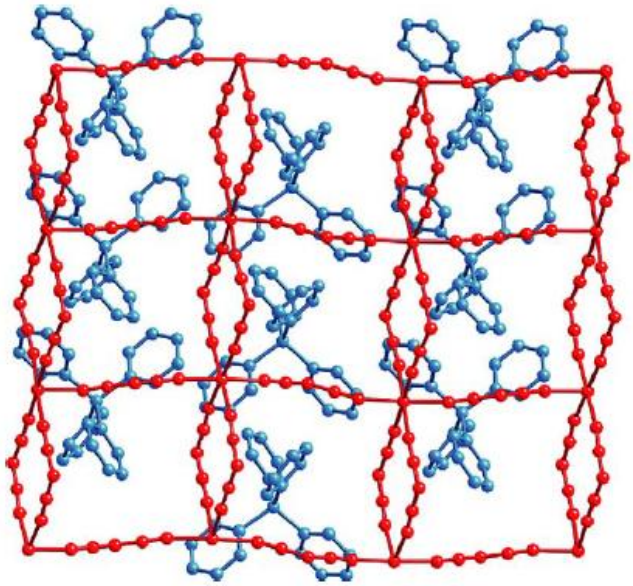

Figure 12. 2D topology of $(Ph_4E)Mn(dca)_3$[10]

The anionic layers formed by metal-dicyanamide alternate with $(Ph_4E)^+$ cation layers. Columns created by cations are interconnected by π-π interactions.

Phenyl groups of cation can be replaced by alkyl substituent disrupting intercation supramolecular interactions. Substitution of smaller $(MePh_3P)^+$ cations into network has two effects. First, substitution of smaller $MePh_3P^+$ disrupts the cation-anion and cation-cation interactions. Second, $Mn(dca)_3^-$ network is not flexible enough to insert smaller cations without reducing the packing efficiency of cation layer.[2] These effects change the network of $(MePh_3P)Mn(dca)_3$ from 2D to 3D as illustrated in Figure 13.

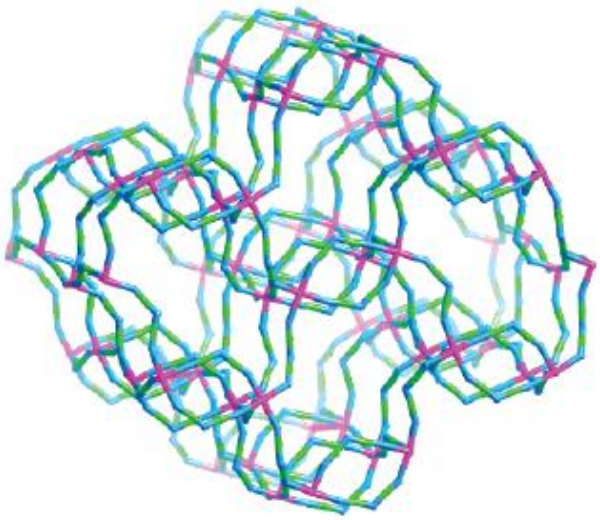

Figure 13. 3D topology $(MePh_3P)Mn(dca)_3$

The 3D network of $[Mn(dca)_3]^-$ includes singly and doubly bridged metal atoms that are connected to sheets by single dicyanamide bridges from above and below, which forms a 3D network with hexagonal channels. The smaller $(MePh_3P)^+$cation lie in pairs within the network cavities rather than discrete layers as seen in the $(Ph_4E)Mn(dca)_3$ network. In summary, the anionic pseudohalide dcyanamide is an excellent versatile ligand in the formation of engineered networks. Modification of metal-dicyanamide network by introduction of coligands or cation templation make the network possible to design a diverse range of crystal structures with different physical properties.

1.3. Metal-Dicyanamides as Solid Adsorbents

Dicyanamide is a versatile ligand and it can coordinate to metal ion in many different ways. The network of metal dicyanamide compound can be enlarged inserting ligands into structure. Until now, metal dicyanamide compounds are widely studied and new compounds with different structures were synthesized. Metal dicyanamide network with coligands are widely studied in the field of magnetism; however, selective gas sorption studies were not so popular until 2014. $[Cd(\mu\text{-hmt})(\mu\text{-dca})_2]$[24,25] was studied for its gas sorption ability. Although Cd is a heavy metal, the porous nature of metal dicyanamide network is utilized in the study. In addition, $M(dca)_2(H_2O)_n hmt_n$ (M=Co, Mn) compound have also been studied.[11] It is, however, not appropriate for gas adsorption because of the coordination of water molecules to metal ions resulting in the collapse of the network under vacuum.

1.4. CO_2/N_2 Separation

In the recent years, fossil fuels have been extensively used over centuries, but the reserves of these fossil fuels are depleting rapidly.[26–29] Moreover these fuels have serious impact on the environment like hazardous greenhouse gases emission, change in atmospheric equilibrium.[30–34] CO_2 release has dramatically increased mainly because of the consumption of fossil fuels and CO_2 increased the air toxicity and ocean acidity.[35,36] To decrease the global warming, the selective capture of CO_2 has gained an interest in the world. In the industry, post-combustion CO_2 capture with air separation is crucial for a better sustainable low carbon future; therefore, CO_2 needs to be captured by adsorbents. The capturing is affected by surface volume, adsorption enthalpy and

functional groups inside the pores.[37–41] Creating polarizing groups in the pores, like nitrogen based one, essentially increases the selective adsorption of CO_2. Creating accessible nitrogen atoms inside the pores is an effective way to increase CO_2/N_2 selectivity. The Lewis acid characteristic of CO_2 with nitrogen donor sites increases the CO_2 uptake capacity and selectivity by dipole-quadrupole interactions between the available nitrogen atoms and CO_2. This fact has been utilized in many studies.[42,43,44] For example, SBA-15 surface basicity was changed by nitrogen base molecules like amines and imidazole and CO_2 was used to characterize basic sites. Coordination of CO_2 with basic sites results in the decrease of activation energy and so inert molecules can be turned to functional products.

1.5. Literature View for Water Oxidation Catalyst

In the world, the need for energy is dramatically increasing with sharp increase in the CO_2 level. To overcome the negative effects of the CO_2 level, synthetic photosynthesis approach must be developed. Over the past few decades, many research groups have been working on perfecting the art of mimicking the photosynthesis process of splitting water to generate energy.[45–47] Water is a sustainable and affordable source of hydrogen, but O-H bond cleavage is an energetic process.[48] Conversion of solar energy into chemical energy in form of carbon-based molecules by splitting water molecules in photosynthesis is a well-defined by the association of the pigment chlorophyll. The whole procedure works on the association of an electron acceptor and an electron donor.[49,50] Water splitting is not so easy process, the process requires two catalysts: One of them is to split water into O_2 and the other catalyst is for H_2 formation via reduction

of protons. As seen in the detailed oxidation and reduction process, oxidation of water into O_2 requires high oxidation potential.[51]

$2H_2O \rightleftharpoons O_2 + 4e^- + 4H^+$ $\quad E_{anode} = 1.23 - 0.059\times(pH)$ V (vs. NHE at 25°C)

$4e^- + 4H^+ \rightleftharpoons 2H_2$ $\quad E_{cathode} = 0 - 0.059\times(pH)$ V (vs. NHE at 25°C)

The overcome the high kinetic barrier, water oxidation catalyst needs to be synthesized and they need to be stable, cheap and work in low overpotential. For this reason, many researchers focused on water oxidation catalyst.

As a water oxidation catalyst (WOCs), cobalt based one with high catalytic activity and diversity has gained an interest. Oxide and non oxide forms of cobalt base WOCs are widely studied in this field. One of the most important studies in the oxide form of cobalt based WOCs belongs to Daniel G. Nocera.[52] In the study, as an electrode indium tin oxide was used and cobalt phosphate thin film synthesized from phosphate buffered cobalt(II) solution. The metal oxides as water oxidation catalyst showed high catalytic activities and they required sensible overpotential and concentrated basic solutions. However, creating a catalysis working at pH 7 with low potential is problematic and many catalysts do not operate in neutral water within the ambient conditions.[52] Over the past few years, non-oxide systems have been of greater emphasis. Various cobalt-based non-oxide systems such as cyanide systems[53–55] and carbodiimides[56] are reported to be efficient and robust catalysts. Non-oxide catalysts including Co-Fe Prussian Blue networks have been synthesized.

As heterogeneous water oxidation catalysis, this network has advantages over oxide forms of WOCs such as robustness and stability in both neutral and acidic media. Although, non-oxide forms of WOCs have advantages, the low current density because of the low surface concentration is their main disadvantage. To overcome the drawback of the non oxide ones, a study was recently performed.[52] In the study, for preparation of Co-Fe coordination polymers, synthetic pentacyanometalate-based metallopolymer was used and increase in surface concentration with increase in the catalytic activity was observed.

One of the other important studies belongs to Galán-Mascarós research group. In the study, cobalt hexacyanoferrate (CoHCF) Prussian blue type cyanide bridged coordination polymer is used for electrocatalytic water oxidation. They investigated the catalytic activity of CoHCF and compared it with cobalt oxides. The TOF value 2.6×10^{-3} s^{-1} was observed at $\eta = 410$ mV for cobalt oxides while it is $\eta = 305$ mV for CoHCF, which showed that the water oxidation performance of CoHCF is comparable to those of cobalt oxides.[53] The other study in the field of water oxidation catalysis is related to cobalt carbodiimide by Patzke research group.[57] Compared to the oxide form, carbon and nitrogen based ones are more stable, oxide free, and include positively polarized carbon active sites with nitrogen. Over the years, the demand for water oxidation catalyst has been increasing. As seen in the studies, catalytic activities of cyanied bridged CoHCF and cobalt carbodiimide have been studied. In this thesis, catalytic activities of cobalt dicyanamide compounds are investigated in the field of water oxidation catalysis.

Chapter 2

EXPERIMENTAL

2.1. The Synthesis of Co(hmt)$(dca)_2$ for CO_2/N_2 Selectivity

In the synthesis of the new microporous metal dicyanamide compound, all chemicals and solvents were purchased from Aldrich and used without further purification. Firstly, a starting material $Co(NO_3)_2.6H_2O$(1g,3.43mmol) dissolved in methanol. Hexamethylenetetramine (hmt) and sodium dicyanamide also dissolved in methanol solution separately. When all chemicals were dissolved completely, methanol solutions of hmt and sodium dicyanamide were slowly added to the methanol solution of $Co(NO_3)_2.6H_2O$ to obtain the 1:1:2 (Co:hmt:dca) stoichiometric ratio in the mixture. The mixed solution was stirred for 24 hours and then filtered. After precipitation, a red powder precipitate was obtained and the precipitate was washed with distilled water and methanol. The precipitate was kept at 60^oC for drying and the yield is 27%. To synthesize fine crystals of the compound, $Co(NO_3)_2.6H_2O$ (25 mg, 3.43 mmol) was dissolved in a 30 mL methanol solution. The methanol solution of $Co(NO_3)_2.6H_2O$, slowly layered with the 30 mL methanol mixture of hmt and sodium dicyanamide. After three weeks, red crystals were obtained.

2.2. The Synthesis Pathway of Electrodes for Water Oxidation Catalyst

All the chemicals were purchased from Sigma-Aldrich and water with 18 MΩ resistivity used during the preparation of solutions. In the water oxidation catalyst study, eight

different combinations of materials were synthesized which are: $Co(dca)_2$,$Fe(dca)_2$, $Ni(dca)_2$, $Co_{0.5}Ni_{0.5}(dca)_2$, $Co_{0.9}Ni_{0.1}(dca)_2$, $Co_{0.5}Fe_{0.5}(dca)_2$, $Co_{0.9}Fe_{0.1}(dca)_2$, and $Co_{0.9}Fe_{0.05}Ni_{0.05}(dca)_2$. All materials were coated onto fluorine doped tin oxide (FTO) via drop-casting method. The conductive working electrode FTO is 1x2 cm, 2 mm thickness with 7 Ω/sq surface resistivity. The procedure for the coating of the catalyst onto an FTO electrode is the same for each materials listed above. Before coating, FTO electrode was cleaned for 10 minutes in basic soapy solution, deionized water and lastly isopropanol. After that, FTO glasses were annealed for 30 minutes at 400^{o}C for a more hydrophilic surface. The buffer solutions were prepared from K_2HPO_4 and KH_2PO_4, the pH was changed using H_3PO_4 and KOH. To prepare the catalyst, dicyanamide was dissolved in DMF solution and slowly added into water solution of metal salt in a stoichiometric ratio 1:2:2 (M^{2+}: dca: DMF). The resulting suspension was stirred for all day and then filtered. The precipitate was dried over the night at 60^{o}C and prepared for the electrochemical studies. To prepare catalyst modified electrodes, 5 mg catalyst, 1 mL DMF, and 100 μL Nafion were used and sonicated for 30 minutes. After sonication, 50 μL of the mixture was dropped onto a clean FTO electrode only in 1x1 cm and the rest of the surface masked with a polymeric band. Then, the electrode was dried at 80^{o}C for 10 minutes. Before the analysis, the electrode needs to be washed with deionized water. Cyclic voltammograms (CV) were recorded with a scan rate of 50 mV/s in 50 mMKPi (pH 7) containing 1 M KNO_3 as electrolyte between 0 V and 1.5 V (vs Ag/AgCl). All experiments were carried out under nitrogen atmosphere.

2.3. Instrumentation

2.3.1. Fourier Transform Infrared Spectroscopy (FTIR)

Fourier transform infrared spectra (FTIR) in transmission mode were recorded by Bruker ALPHA Tensor 27 model. As a detector, a Digi Tech TM DLATGS with a 4.0 cm^{-1} resolution was used. The spectra were recorded by 64 scans in the range of 400-4000 cm^{-1}.

2.3.2. Powder X-Ray Diffraction (PXRD)

X-ray diffraction studies were performed using Miniflex Rigaku diffractometer with Cu Kα X-ray radiation. The diffaction pattern were collected in the 2θ diffraction angel with a range of 3-63°, step size of 0.01 and a scan rate of 1° min^{-1}. For the powder samples the crystalline behavior PANalytical's X'Pert Powder X-ray diffractometer (Multiple Purpose Diffractometer) was also used with a CuKα X-ray source .

2.3.3. Single Crystal X-Ray Diffraction

The data was collected using Rigaku MicroMax 007HF diffractometer with a monochromatic Mo Kα radiation. The crystal, suspended in polybutene oil, was placed on a holder and the data taken from Rigaku CrystalClear software one. The data indexed to orthorhombic unit cell and it indicated the space group as *Pnma*. To solve the crystal structure, SHELX suite of programs and Olex2[58] was used.

Metal atoms, hydrogen and non-hydrogen atom positions were placed in the crystal structure and CrystalMaker program was used to illustrate crystal structures.

2.3.4. Thermogravimetric Analysis (TGA)

In the thermogravimetric analysis of the sample, TA Instruments TGA Q500 Model was used. Measurement was performed under N_2 atmosphere, 10^oC/min from 30 to 500^oC.

2.3.5. CHNS/O (Elemental) Analysis

Elemental analysis measurements performed by Thermo Scientific FLASH 2000 CHNS/O Analyzer.

2.3.6. Scanning Electron Microscopy (SEM) and Energy Disperse X-Ray Analysis (EDX)

Scanning electron microscopy (SEM) imaging was performed at beam voltage 5 kV and Energy-dispersive X-ray spectroscopy (EDX) analysis was carried out at 30 kV using FEI-Quanta 200 FEG ESEM.

2.3.7. Gas Adsorption Measurements

The gas adsorption data taken from Micromeritics Tristar 3000 surface area and pore size analyzer to perform N_2 adsorption studies at 77 K to obtain surface area.

2.3.8. X-Ray Photoelectron Spectroscopy (XPS)

In order to detect the elements and the oxidation states, Thermo Scientific K-Alpha X-Ray Photoelectron Spectrometer system operating with Al Kα micro-focused monochromator source (hν-1486.6 eV & 400 mm spot size) along with a flood gun for charge neutralization, pass energy 200 eV was used for survey scan and 30eV individual element scans.

2.3.9. Electrochemical Mesurements

The electrochemical measurements were performed at room temperature by Gamry Instruments Interface 1000 Potentiostat/Galvanostat. In the experiment; reference, counter and working electrode were used. As a reference electrode, Ag/AgCl electrode saturated with 3.5 M KCl, a Pt wire as counter electrode and a modified fluorine doped tin oxide was used as a working electrode. In the experiment, 50 mM potassium phosphate buffer solution (KPi, pH7) including 1 M KNO_3 was used as electrolytes. Buffer solutions were prepared by K_2HPO_4 and KH_2PO_4. H_3PO_4 or KOH was used to change pH. During cyclic voltammetry and chronoamperometry measurements, the system including counter and reference electrodes was bubbled with N_2 gas to remove dissolved oxygen gas. When nitrogen gas was removed from the system, the working electrode was inserted into the system for the measurement.

Chapter 3

RESULTS AND DISCUSSION FOR METAL DICYANAMIDES AS SOLID ADSORBENTS FOR CO_2/N_2 SEPARATION

3.1. STRUCTURAL CHARACTERIZATION

This study, performed by our group was published.[59] The crystal data indicates the space group as *Pnma* and shows an orthorhombic unit cell. The data related to $Co(hmt)(dca)_2$ crystal structure is shown in Table 1.

Table 1. The crytal data for $Co(hmt)(dca)_2$

$[Co(hmt)(dca)_2].H_2O$	
Empirical Formula	$C_{10}H_{14}CoN_{10}O_1$
Space group	P_{nma} (No. 62)
Formula Weight	349.24 g/mol
Unit Cell : *orthorhombic*	a=12.5771(3) Å, b=12.1488(3) Å, c=10.3245(3) Å
Unit Cell Volume	1577.55(7) $Å^3$
Z	4
Density, ρ_{calc}	1.470 g/cm3
abs. coeff., μ	1.106 $mm^{-}1$
Crystal color and habit	Red block
Crystal size	0.4 x 0.5 x 0.6 mm^3
Temperature (K)	293
Radiation, λ	Mo Kα, 0.71075 Å
Min. and max. θ	2 - 27.5^o
Reflns collected	4643
Independent reflns	1182
Data/parameters/restrains	1882/132/0
R [Fo > 4σ(Fo)]	R_1 = 0.0351, wR_2 = 0.1078

According to the X-ray structural data, a 3D coordination network of Co(hmt)$(dca)_2$ is illustrated in Figure 14. In the inversion center Co(II) is placed and metal ion are connected by hmt and dicyanamide bridging ligand. In the structure, each Co(II) metal center linked to six nitrogen atoms. Four of the nitrogen atoms belong to terminal nitrogen atom of dicyanamide anion and two of them belong to hmt groups.

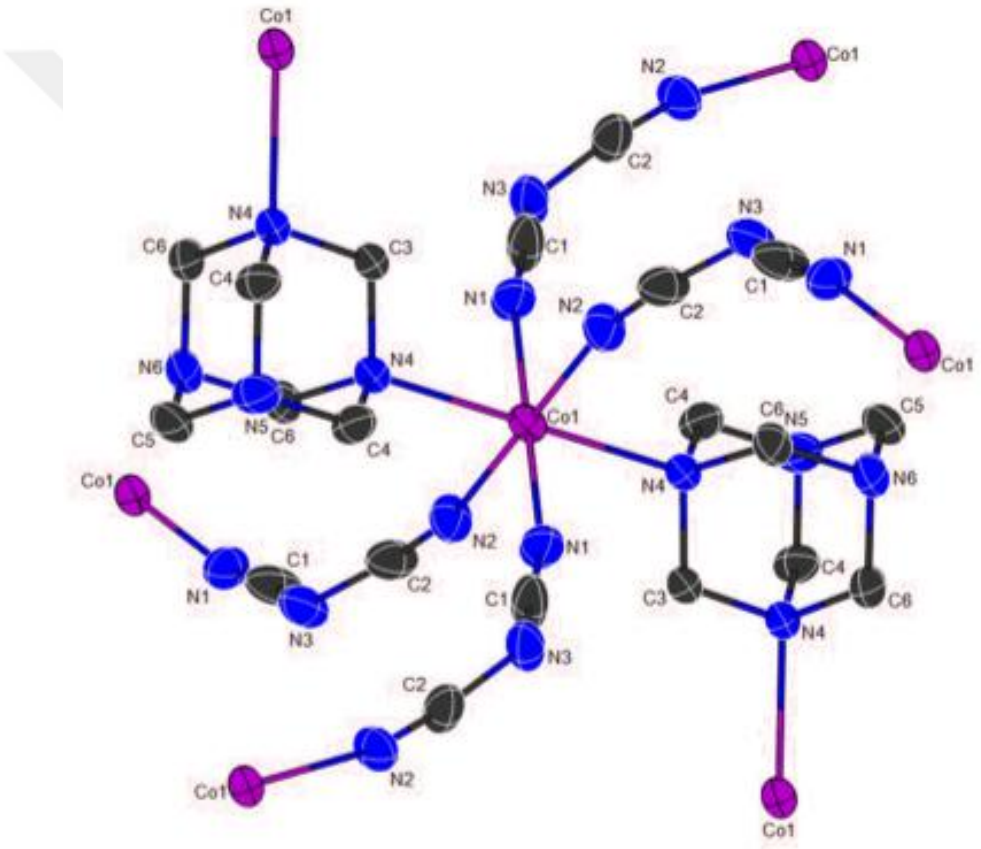

Figure 14. Cobalt center coordination and binding ways to hmt and dicyanamide (Hydrogen atoms are not illustrated for the sake of simplicity)

In the structure of the coordination modes of Co(II) center, bindings to metal ion form a distorted octahedral geometry as shown in Figure 14. In the dicyanamide binding, nitrile nitrogen atoms are used and $\mu_{1,5}$-dca type of bonding is observed. In the 2D layer of $Co(dca)_2$, each dicyanamide is linked to two metal centers with a distorted square geometry as illustrated in Figure 15.

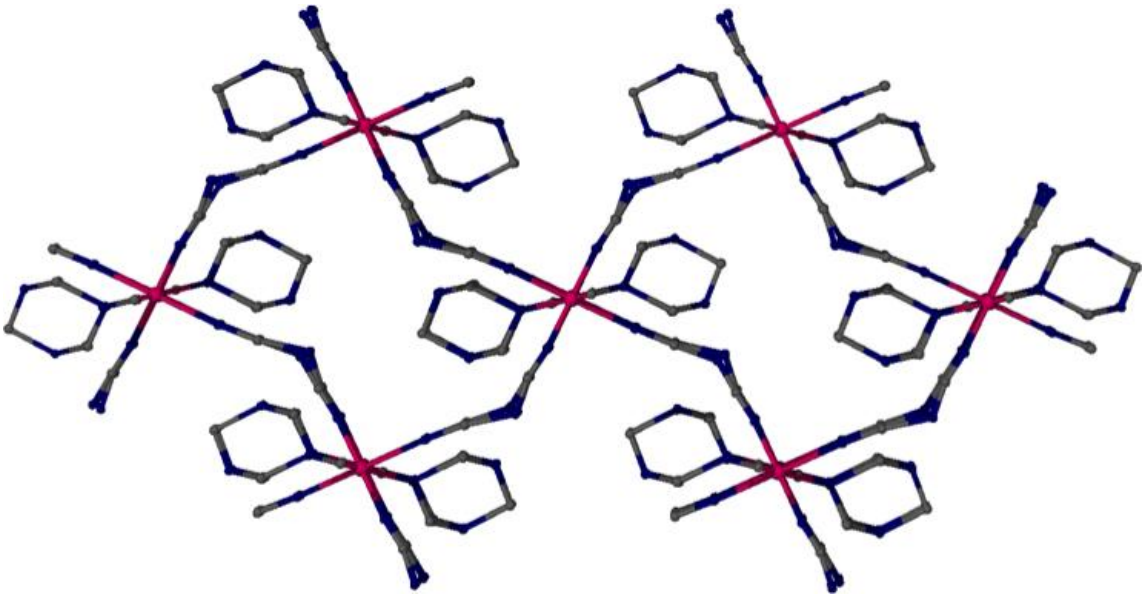

Figure 15. 2D illustration of $Co(dca)_2$ connected by hmt groups (Hydrogen atoms are not illustrated for the sake of simplicity.)

The 2D array of $Co(dca)_2$ is connected to each other by hmt groups and a 3D network structure is described as shown in Figure 16. The space filling diagram is illustrated in Figure 17. In the network, only two of the four nitrogen atoms of one hmt ligand for binding to metal center was used for binding to metal center while remaining two nitrogens are free.

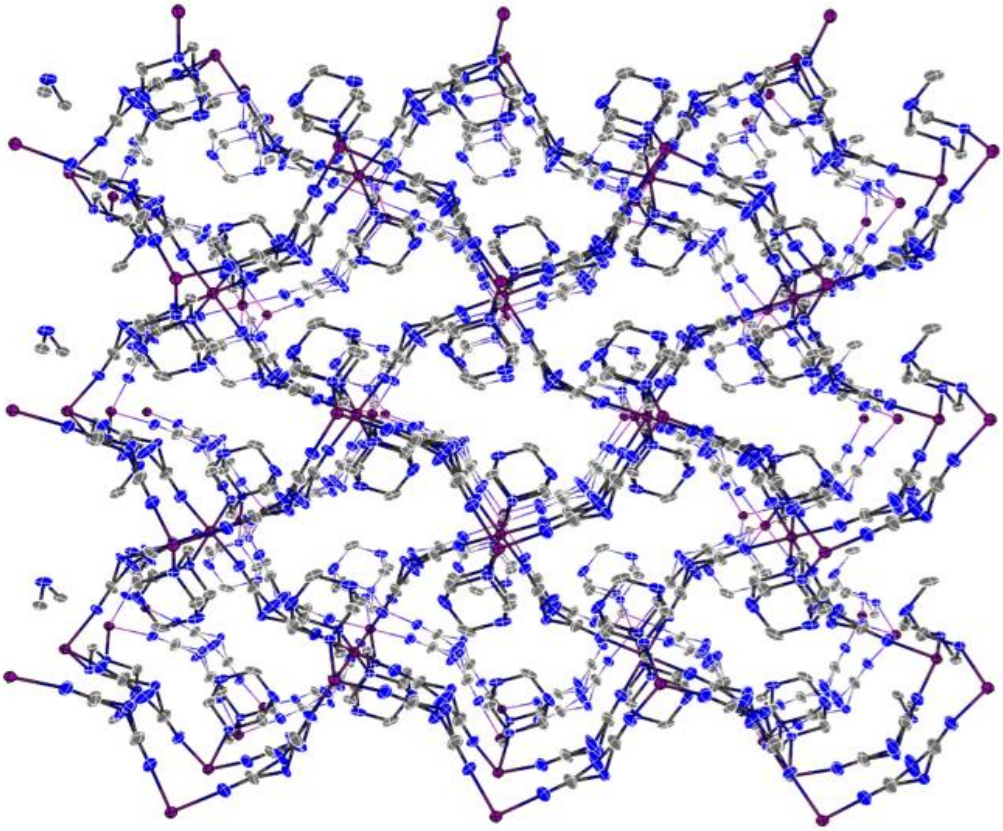

Figure 16. 3D illustration of Co(hmt)$(dca)_2$ (Hydrogen atoms and solvent molecules are not illustrated for simplicity.)

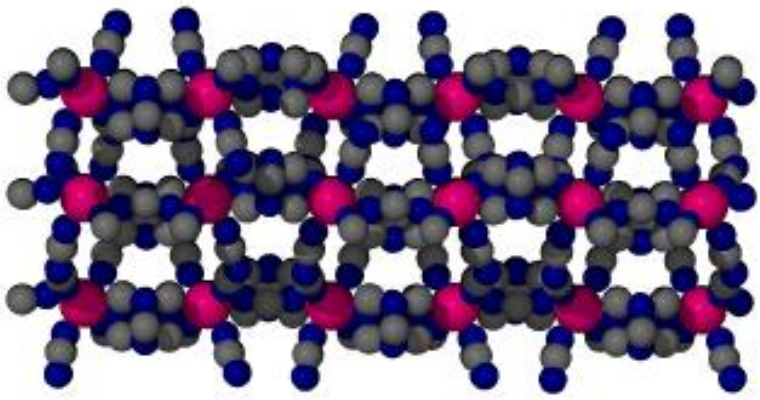

Figure 17. Space filling diagram of Co(hmt)$(dca)_2$ (Hydrogen atoms and solvent molecules are not illustrated for simplicity.)

In the Co(hmt)$(dca)_2$network, selected bond distances and angles are shown in Table 2. Compared to previous studies of metal dicyanamides with hmt ligand[15,25,58] the bond angles and distances are in good accordance.

Table 2. Selected bond distances and angles

Atoms	**Bond Distances Å**
Co1-N1	2.1409(14)
Co1-N2	2.1048(13)
Co1-N4	2.2834(12)
N1-C1	1.170(2)
N2-C2	1.147(2)
N4-C4	1.5410(19)
C2-N3	1.352(5)
C1-N3	1.372(5)
Bond Angles	
N1-Co1-N4	90.32(5)
N2-Co1-N4	88.80(5)
N2-Co1-N1	86.70(6)
C3-N4-Co1	109.07(9)
C4-N4-Co1	112.37(8)
C1-N1-Co1	164.34(14)
C2-N2-Co1	166.14(15)
N2-C2-N3	162.3(5)
C2-N3-C1	117.2(3)
C4-N5-C5	108.29(14)
C6-N4-Co1	110.73(9)

The pore apartures of the crystal in different sizes are illustrated in Figure 18.

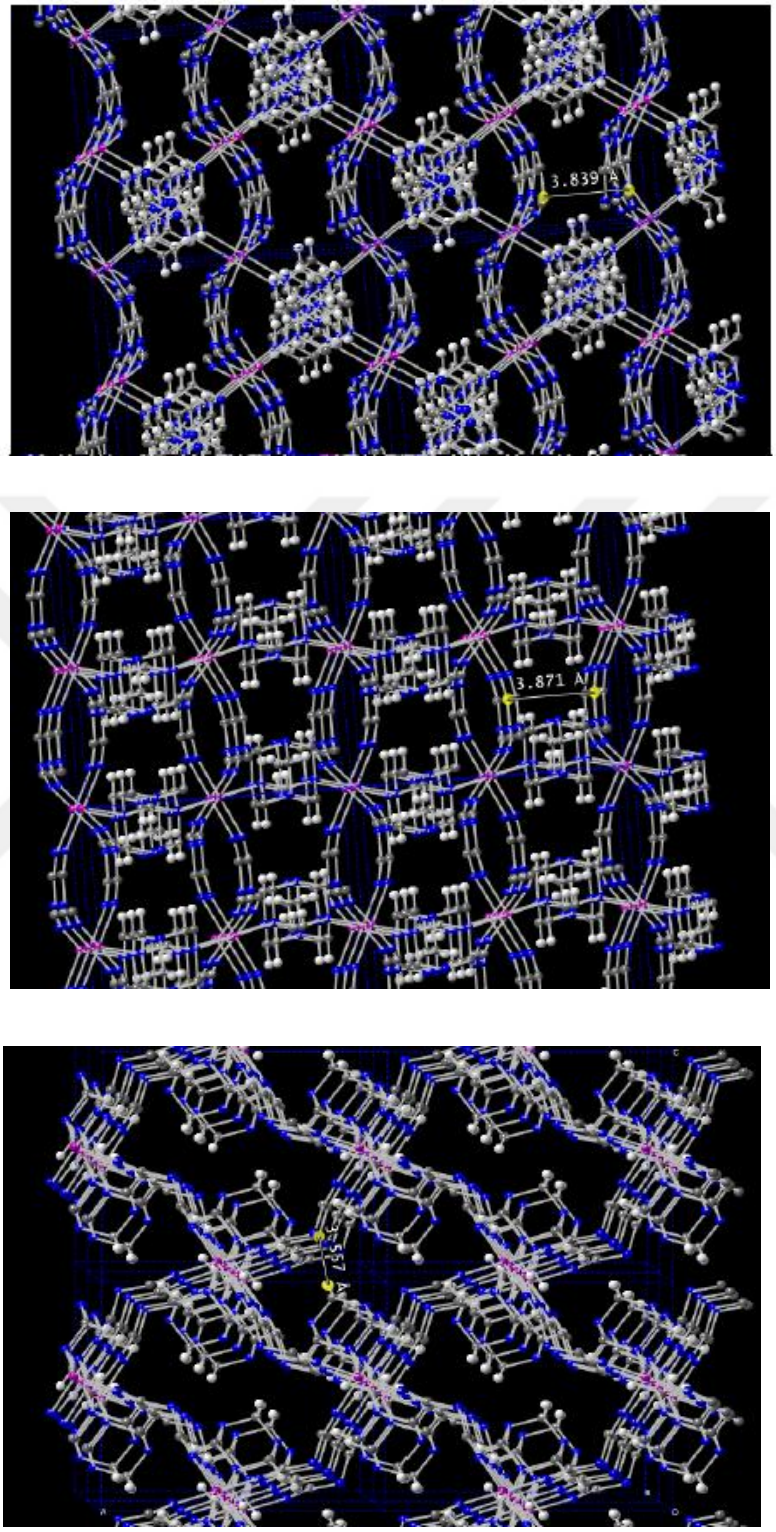

Figure 18. Crystal structure of Co(hmt)$(dca)_2$.

In the thermogravimetric analysis percent weight change started almost at 225°C. The weight change behaviour of the $Co(hmt)(dca)_2$ while increasing in the temperature is shown in Figure 19.

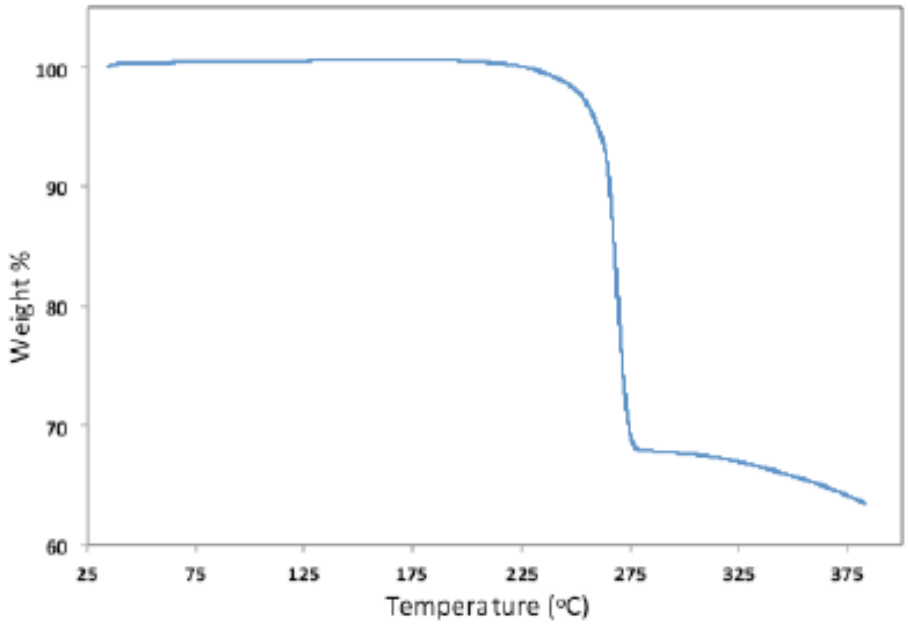

Figure 19. Thermogravimetric analyis of $Co(hmt)(dca)_2$ powder

An infrared spectrum of the compound is illustrated in Figure 20. The spectrum contains three absorptions in the υ(C≡N) region; 2180, 2237, and 2325 cm^{-1} in addition to a stretch at 930 cm^{-1}, which are attributed to the assymmetric and symmetric cyanide stretches of dicyanamide bridging ligands. The compound also shows two strong bands at 1031 and 1236 cm^{-1} and several weak bands in the range 2900–3000 cm^{-1}, which can be assigned to the C-N and aliphatic υ(CH) stretching vibrations of hmt group, respectively.

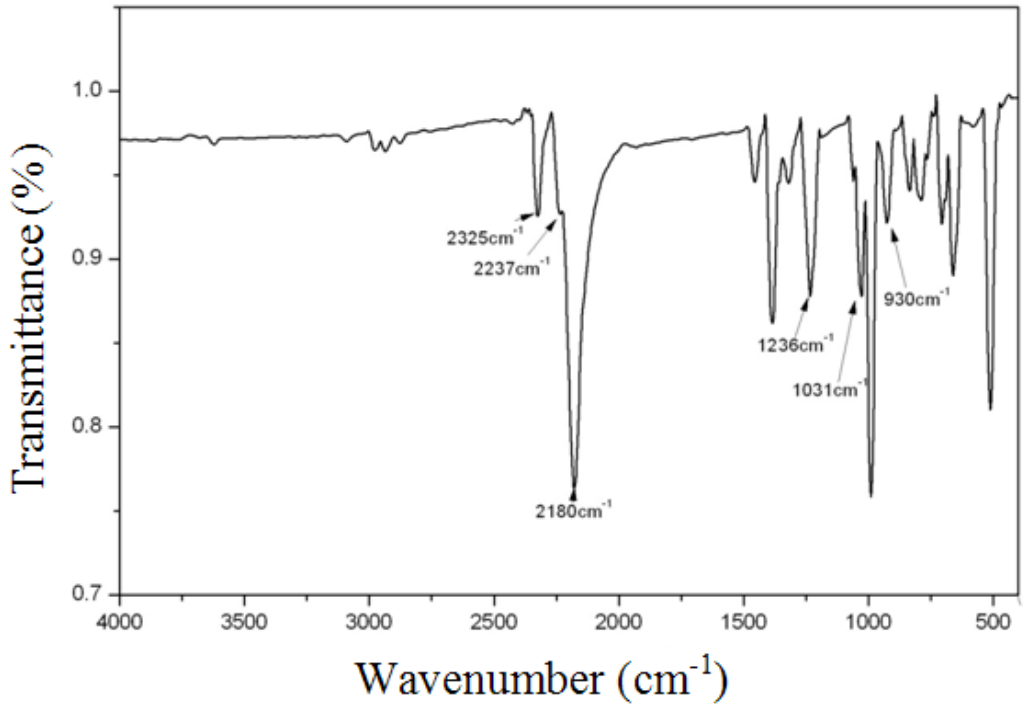

Figure 20. The infrared spectrum of $Co(hmt)(dca)_2$

Elemental analysis of the compound, $Co(hmt)(dca)_2$, $CoC_{10}H_{12}N_{10}$: calculated C 36.26, H 3.65, N 42.29; found C 36.02, H 3.33, N 41.92. Elemental analysis data studied on powder ones indicate that powder samples and crystals are isostructural.

3.2. GAS ADSORPTION STUDIES

For the compound Co(hmt)(dca)$_2$ CO_2 and N_2 adsorption studies were performed until 1 bar at temperatures of 273 and 295 K. The maximum CO_2 loading is 77.3 $cm^3.g^{-1}$ at 273 K and 1 bar and 44.8 $cm^3.g^{-1}$ at 295 K and 1 bar while the isotherms are fully reversible as shown in Figure 21.

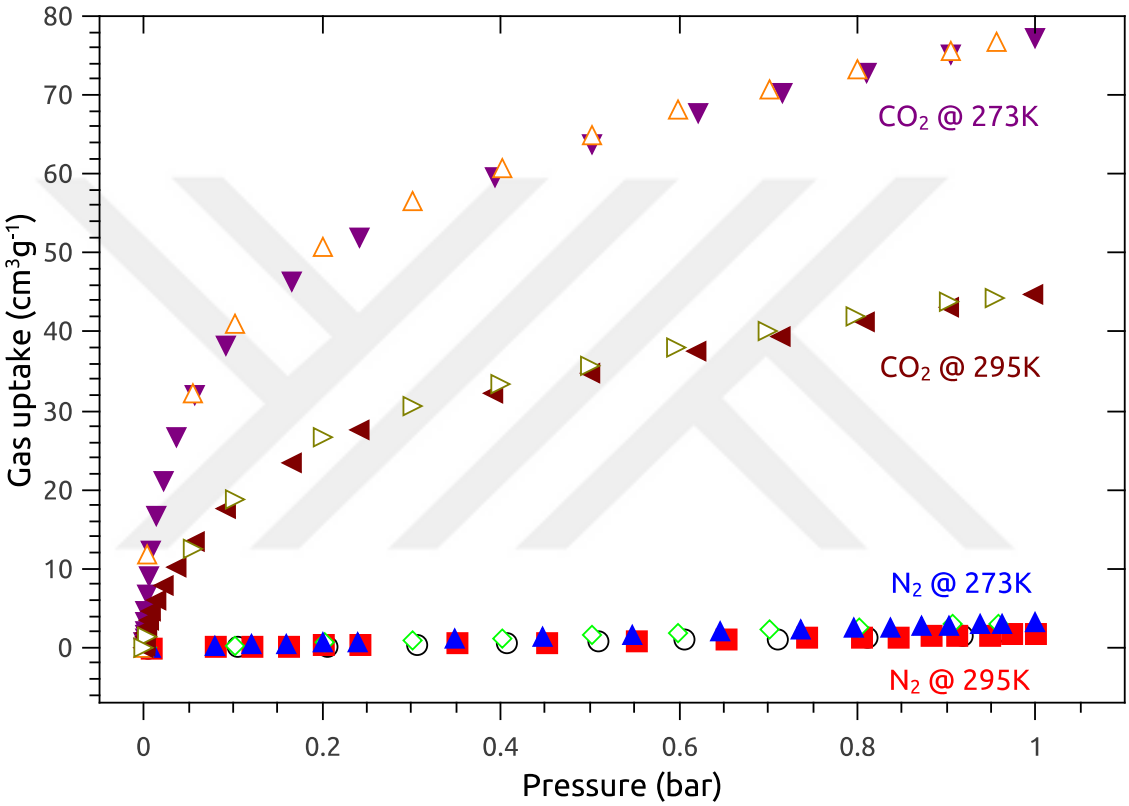

Figure 21. CO_2 and N_2 gas adsorption/desorption isotherms until 1 bar at 273 K and 295 K. Solid symbols show gas adsorption and open symbols show gas desorption.

For the calculation of selectivity and heat of adsorption values; dual site Langmuir model (two available binding sites for the CO_2 molecule),[60] (Figure 22 and Figure 23) are appropriate for the CO_2 isotherms and single site Langmuir model (Figure 24 and Figure 25) are suitable for the N_2 isotherms.

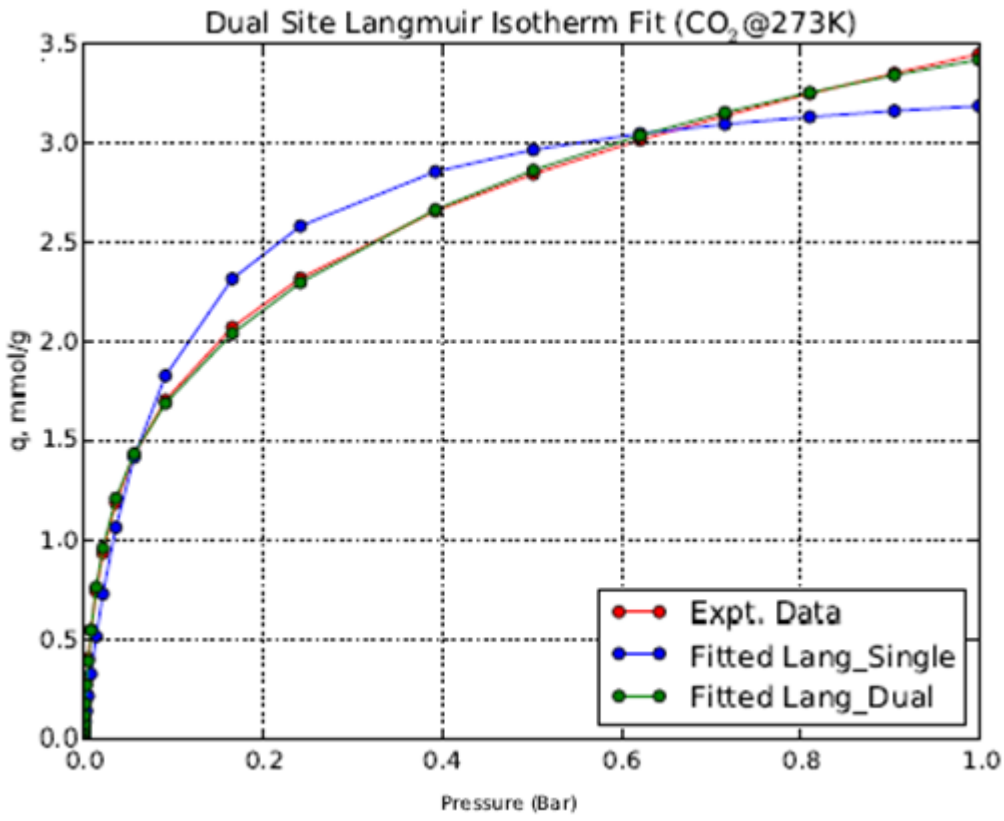

Figure 22. Single and dual site Langmuir isotherms fit for CO_2 adsorption at 273 K

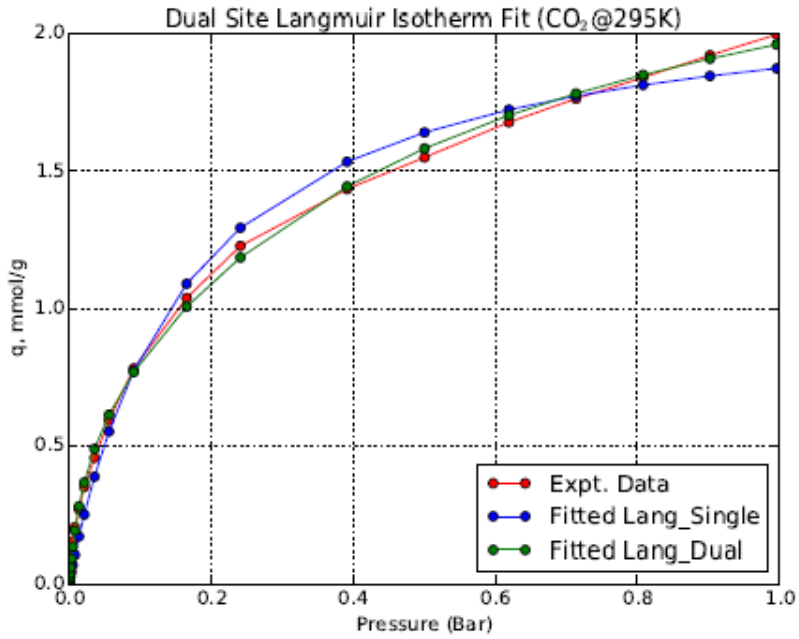

Figure 23. Single and dual site Langmuir isotherm fits for CO_2 adsorption at 295 K

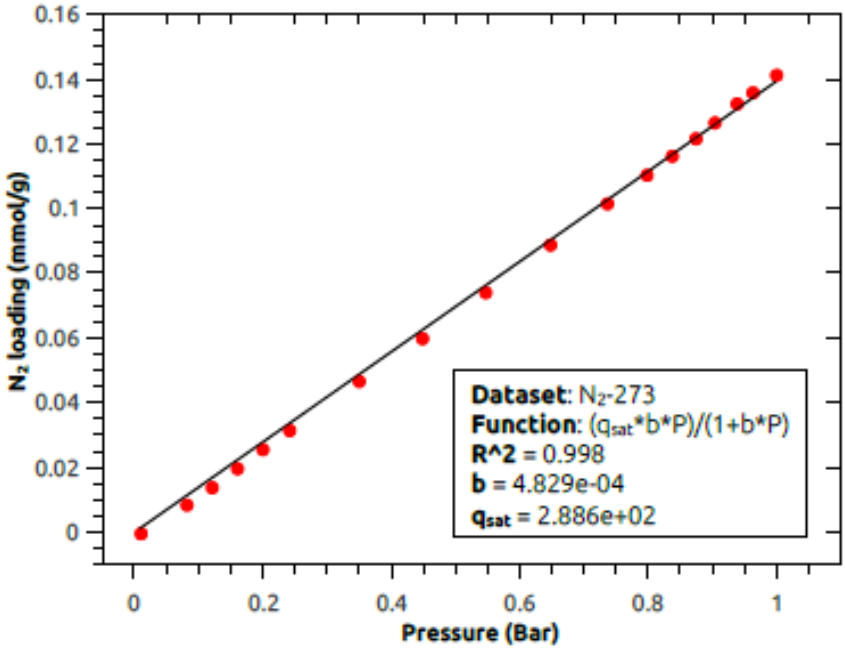

Figure 24. Single site Langmuir isotherm fits for N_2 adsorption at 273 K

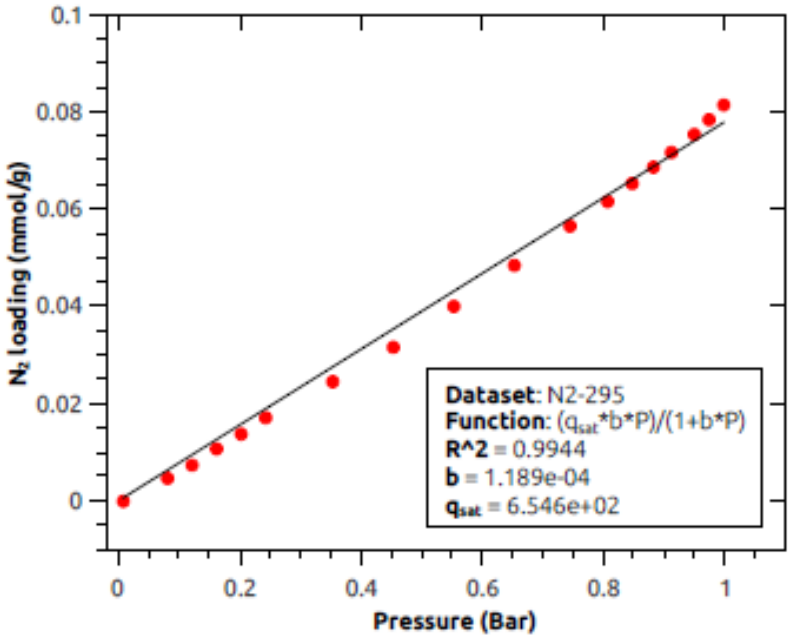

Figure 25. Single site Langmuir isotherm fits for N_2 adsorption at 295 K

The parameters for the single-site Langmuir isotherm and dual-site Langmuir isotherm were reported in the Table 3 and Table 4, respectively.

Table 3. The parameters for single-site Langmuir isotherm

Parameters	N_2–273K	N_2–295K	CO_2–273K	CO_2–295K
q_{sat}	288.7	654.6	3.45	2.19
b	0.0005	0.0001	12.36	6.01

Table 4. The parameters for dual-site Langmuir isotherm

Parameters	CO_2–273K	CO_2–295K
$q_{1,sat}$	1.55	0.57
b_1	57.29	46.79
$q_{2,sat}$	3.12	2.18
b_2	1.58	1.81

The heat of adsorption values were calculated by Clasius-Clapeyron, equation 1, as given below:

$$q_{st} = -\Delta H_{ads} = -R\left(\frac{dlnP}{d\frac{1}{T}}\right) \qquad \text{(Eq. 1)}$$

At low loadings of CO_2, heat of adsorption for CO_2 is 35 kJ mol^{-1}. With the increase in the CO_2 loading after 0.9 mmol g^{-1}, plateau was observed at around 58 kJ mol^{-1} as shown in Figure 26, which can be attributed to two different available binding sites. There are two different N-donor atoms in the compound, each of N atoms belongs to dca and hmt ligands. Thus, dual-site Langmuir isotherm was used for the case of CO_2 adsorption.

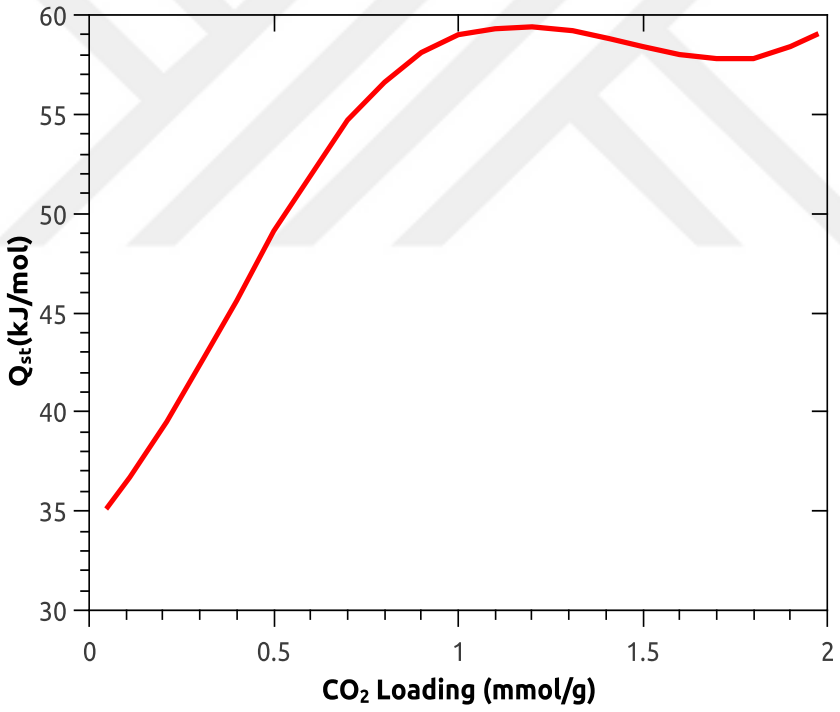

Figure 26. Heat of adsorption with CO_2 loading by dual-site Langmuir isotherms

Unlike CO_2, the heat of adsorption of N_2 as shown in Figure 27 is just 17.7 kJ mol^{-1} and does not change upon N_2 loading.

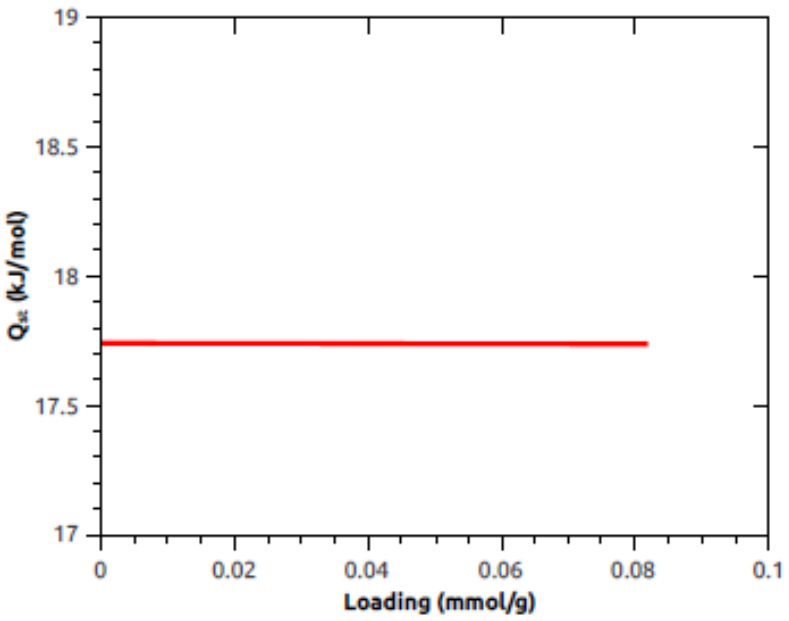

Figure 27. Change of the Q_{st} with N_2 loading by single-site Langmuir isotherms

The CO_2/N_2 selectivity for binary mixtures was calculated by the ratio of the initial slopes and selectivity factor equation as shown in equation 2, loadings from the pure single component isotherm. The selectivity change for the CO_2:N_2 15:85 is illustrated in Figure 28.

$$S = \frac{x_1/y_1}{P_1/P_2} \quad \text{(Eq.2)}$$

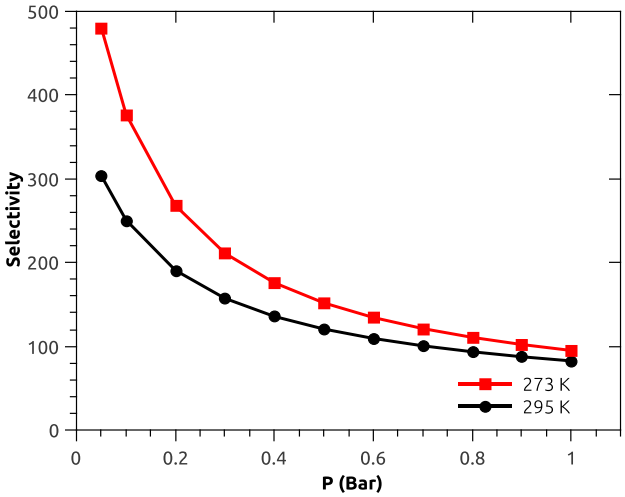

Figure 28. Change in the CO_2 over N_2 selectivity with pressure (CO_2:N_2 15:85)

The CO_2:N_2 15:85 selectivity was determined to be 95 at 273 K and 83 at 295 K and 1 bar. A decrease in the CO_2/N_2 selectivity was observed with the increase of the gas mixture pressure.

The selectivity from the ratio of initial slopes that is obtained by Henry's law ratios is illustrated in Figure 29.

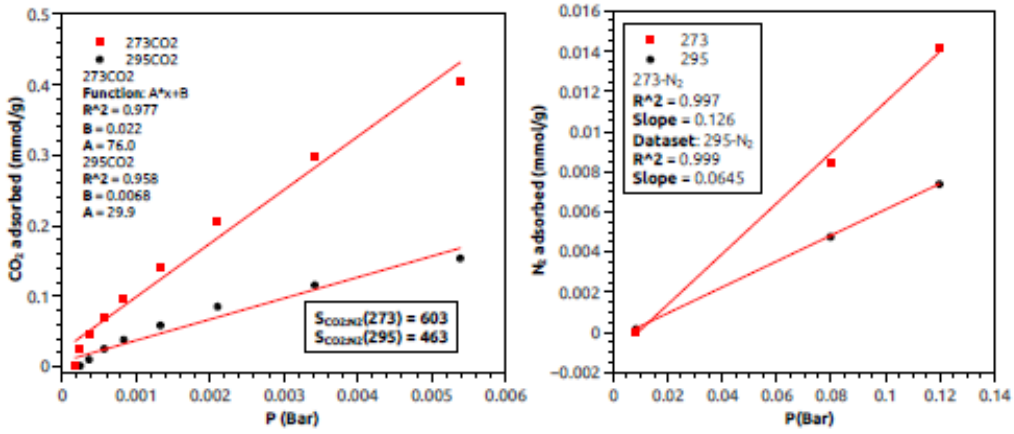

Figure 29. Adsorption selectivity of CO_2 over N_2 by ratio of initial slopes, Henry's constants.

The selectivity obtained from low loading site of the single adsorption isotherms are 603 and 463. The higher adsorption enthalpy of CO_2, thus larger quadrupole with stronger interaction, could be the origin of high CO_2/N_2selectivity. In the crystal, two of the pore openings are around 3.8 Å and kinetic diameter of N_2 is 3.6 Å, CO_2 is 3.3 Å. The similar kinetic diameter of N_2 results in the limited diffusion of N_2 causing a molecular sieving effect, which contributes to high selectivity.[61,62] In addition, BET surface area is 242 m^2/g, measured by CO_2 sorption at 273 K while nitrogen sorption studies failed at 77 K, which was also observed previously in some of porous compounds.[24,38]

To conclude, a new metal dicyanamide compound, $Co(hmt)(dca)_2$ was synthesized and characterized. The network includes octahedral Co(II) center as well as hmt and dicyanamide groups connected to the metal center. In the dicyanamide group each uses one terminal nitrogen while the other one is free. Each hmt group, however, uses two of its nitrogen atoms while remaining two are free. The available free N-atoms can form a polarizable environment and so high CO_2/N_2 selectivity and high heat of adsorption can be realized.

Chapter 4

RESULTS AND DISCUSSION FOR METAL DICYANAMIDES AS WATER OXIDATION CATALYSTS

4.1. Characterization of Metal Dicyanamides

A series of metal dicyanamides with molecular formulas of $M(dca)_2(DMF)_2$ (M: Co, Ni, and Fe) have been studied as water oxidation catalysts. Characterization of these compounds was performed by X-ray diffraction, Infrared spectroscopy and X-ray Photoelectron Spectroscopy.

4.1.1. Single Crystal XRD studies

Single crystal X-ray diffraction studies performed on fine crystals of the compounds reveal that all of the compounds are isostructural and that each of them crystallizes in a monoclinic system with space group P*21/n*. The asymmetric unit of a $M(dca)_2$ structure contains one M(II) site, two dicyanamide groups, and two DMF molecules. Each metal ion shows distorted octahedral MN_4O_2 coordination environment (Figure 30) from four nitrogen atom of independent dca groups and two oxygen atoms that belong to DMF molecules. Therefore, the crystal structure could be explained as a one dimensional ladder-like double chain coordination polymer (Figure 31). Double–chain frameworks consist of two one–dimensional linear chains, which extend in parallel pairs and, thus, are joined at metal node in a ladder fashion (Figure 32). Two ligands adopt certain configuration to connect two metal centers in such a way to form rectangular units (Figure 33).

All of the metal sites coordinated N and O distances are within normal range of statistical errors. The supramolecular framework is stabilized by H••••N interactions [2.555(5) − 2.686(5) Å] originating from the H−atoms of coordinated DMF molecules and central N atom of dca groups. The details of crystal structures are represented in Table 5. Selected bond angles and bond lengths are listed in Table 6.

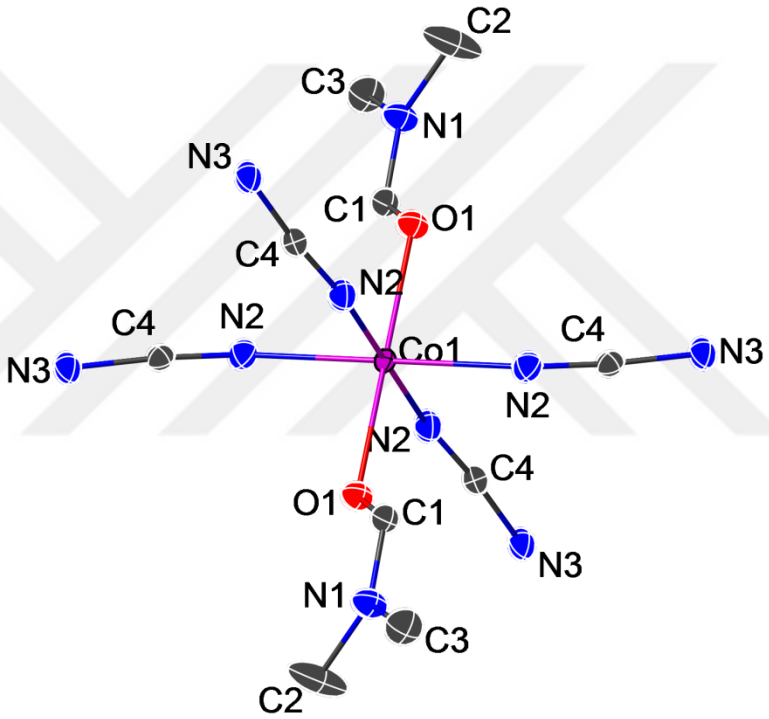

Figure 30. Fragment of the crystal structure of $Co(dca)_2(DMF)_2$ depicting the MN4O2 coordination sphere for metal site. Thermal ellipsoids are projected at the 50% probability level. Hydrogen atoms are not shown for the sake of clarity.

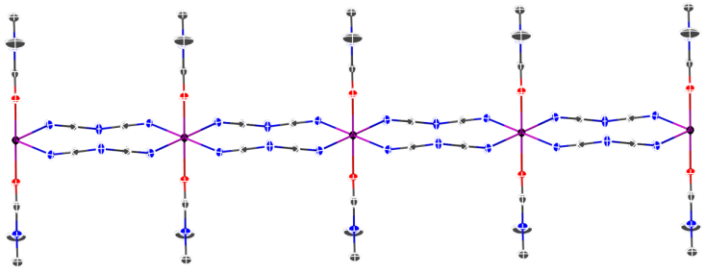

Figure 31. 1D chain structure of $Co(dca)_2(DMF)_2$. Colour code: Co = purple; O = red; C = grey; N = blue. Thermal ellipsoids are projected at the 50% probability level. Hydrogen atoms are not shown for the sake of clarity.

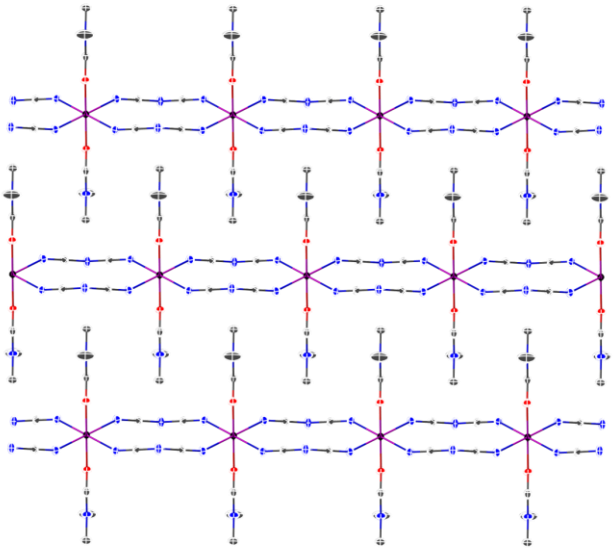

Figure 32. Packing diagram of $M(dca)_2(DMF)_2$ depicted along the a axis.

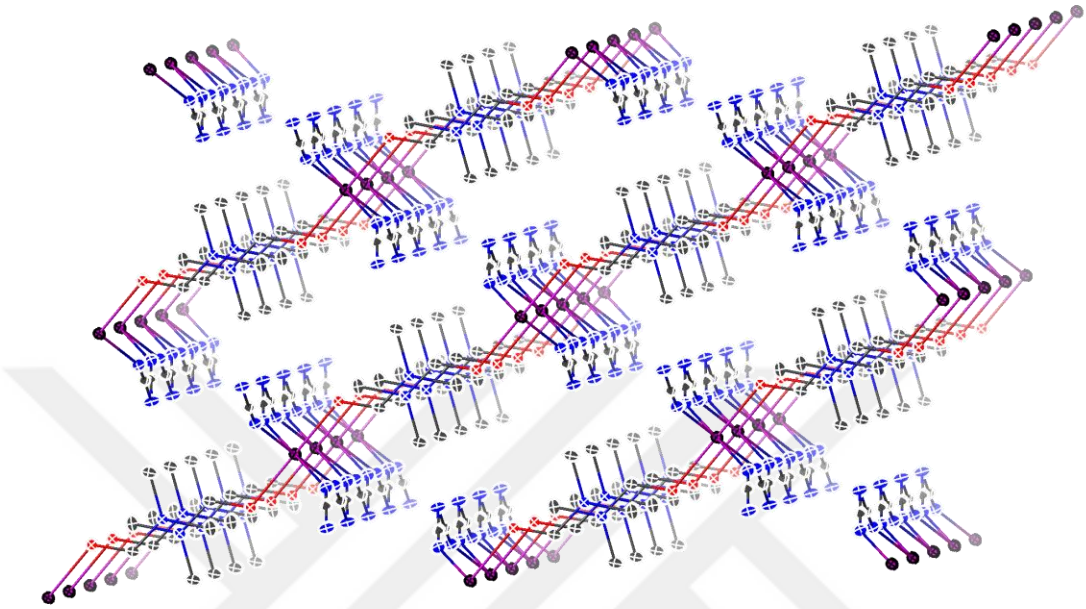

Figure 33. Packing diagram of $M(dca)_2(DMF)_2$ depicted along the c axis.

Table 5. Crystal and Structure Refinement Data

Compound	$Fe(dca)_2(DMF)_2$	$Co(dca)_2(DMF)_2$	$Ni(dca)_2(DMF)_2$
Formula	$C_5\ H_7\ Fe_{0.50}\ N_4\ O$	$C_5\ H_7\ Co_{0.50}\ N_4\ O$	$C_5\ H_7\ N_4\ Ni_{0.50}\ O$
Formula weight	167.07	168.61	168.50
T, K	100(2)	100(2)	100(2)
System	Monoclinic	Monoclinic	Monoclinic
Space group	I2/m	I2/m	I2/m
a, Å	8.061(5)	8.061(5)	8.061(5)
b, Å	7.319(5)	7.319(5)	7.319(5)
c, Å	12.699(5)	12.699(5)	12.699(5)
α (°)	90.000(5)	90.000(5)	90.000(5)
β (°)	103.336(5)	103.336(5)	103.336(5)
γ (°)	90.000(5)	90.000(5)	90.000(5)
V [$Å^3$]	729.0(7)	729.0(7)	729.0(7)
Z	4	4	4
ρ_{calc} [g/cm^3]	1.522	1.536	1.535
μ [mm^{-1}]	1.052	1.195	1.349
F(000)	344	346	348
GOF	1.324	1.151	0.736
Final R indices [I>2σ(I)]	R1= 0.0387 WR2= 0.1080	R1= 0.0339 WR2= 0.0973	R1= 0.0325 WR2= 0.0934
R indices (all data)	R1= 0.0387 WR2= 0.1080	R1= 0.0339 WR2= 0.0973	R1= 0.0325 WR2= 0.0934

Table 6. Selected bond distances (Å) and bond angles (^{o})

	$Fe(dca)_2(DMF)_2$	$Co(dca)_2(DMF)_2$	$Ni(dca)_2(DMF)_2$
M1 O1	2.070(3)	2.070(2)	2.069(3)
M1 N2	2.072(2)	2.071(2)	2.072(2)
O1 M1 O1	180.00(12)	180.00(10)	180.00(10)
O1 M1 N2	91.60(9)	91.58(7)	88.42(8)
N2 M1 N2	92.05(13)	92.07(12)	92.08(12)
O1 M1 N2	88.40(9)	88.42(7)	91.58(8)
N2 M1 N2	87.95(13)	87.93(12)	87.92(12)
N2 M1 N2	180.00(11)	180.00(12)	180.00(18)

4.1.2. Powder X-ray Diffraction Studies of Metal Dicyanamides

X-ray diffraction studies performed on metal dicyanamides show that $Co(dca)_2(DMF)_2$, $Fe(dca)_2(DMF)_2$ and $Ni(dca)_2(DMF)_2$ are isostructural with different degrees of crystallinities as shown in Figure 34. In the XRD pattern, 2θ positions almost overlap each other, which can be attributed to the negligible change in the ionic radius of metals ions.

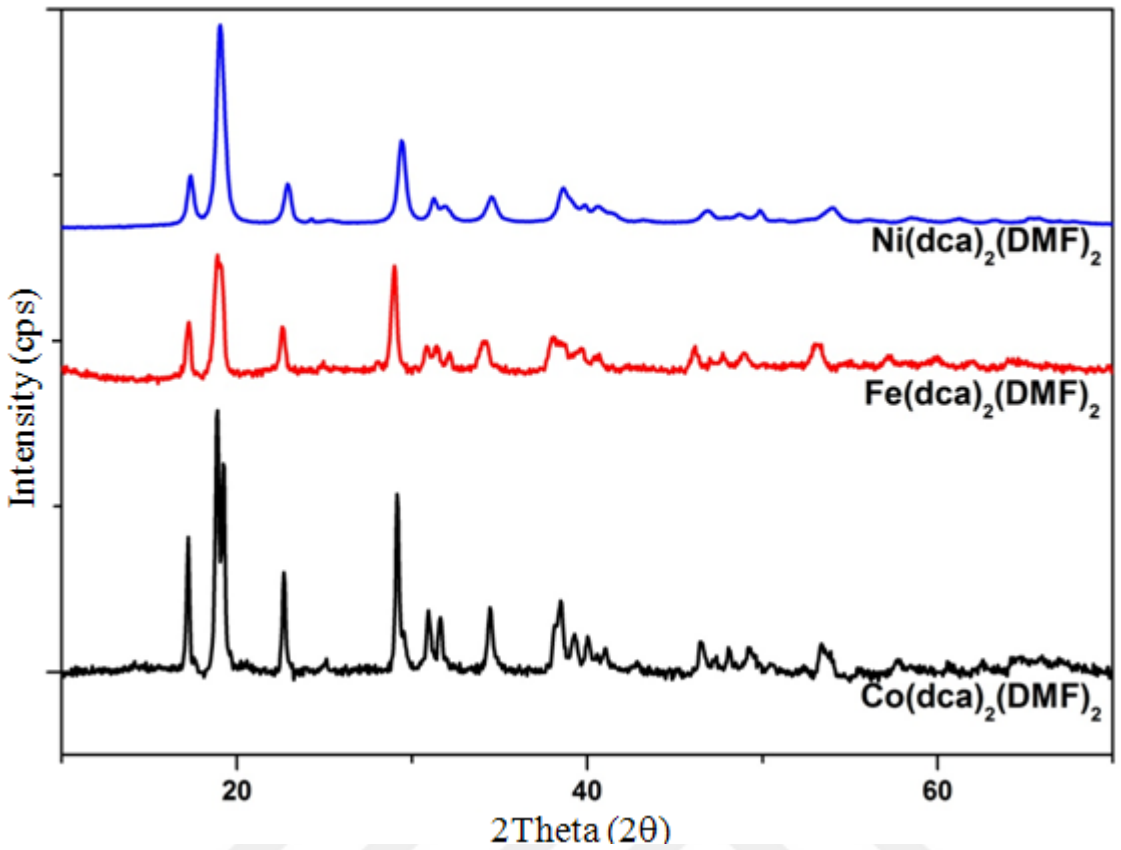

Figure 34. XRD pattern for metal dicyanamides.

4.1.3. Fourier Transform Infrared Spectra of Metal Dicyanamides

In the infrared data as shown in Figure 35, $Co(dca)_2(DMF)_2$ and $Ni(dca)_2(DMF)_2$ illustrate sharp and strong stretching bands while $Fe(dca)_2(DMF)_2$ compound shows broad and weak bands. $\nu_{sym\&asym(C\equiv N)}$ stretches were observed in the wavenumber ranges of 2360 – 2184 cm^{-1}, ν_{asym}(C-N) at around 1380 – 1364 cm^{-1}, and ν_{sym}(C-N) at around 938 cm^{-1}, which can be attributed to the cyanide group in dicyanamide group.[59] Strong bands in the wavenumber range of 1108 – 1015 cm^{-1} corresponding to C-N group, bands at around 1647 – 1640 cm^{-1} can be assigned to the (C=O) stretches, and bands at around 2970 – 2934 cm^{-1} can be assigned to aliphatic ν(C-H) stretching

vibrations of DMF.[63] Presence of a broad stretch at around 3500 – 3250 cm^{-1} in the Fe compound can be due to excess moisture adsorbed, which can also be a reason for the relatively poor crystallinity of the Fe derivative.

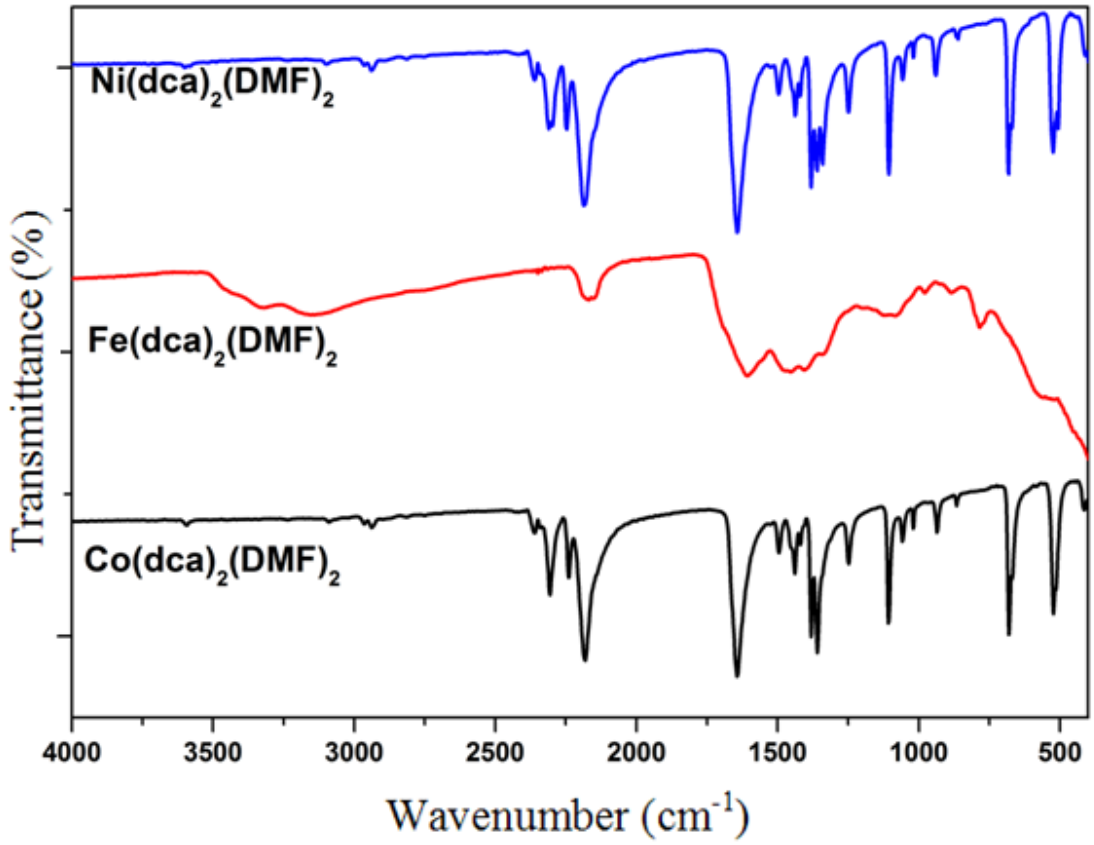

Figure 35. FT-IR spectra of metal dicyanamides compound

4.1.4. X-ray Photoelectron Spectroscopy Studies

XPS analysis was realized for pristine and post-catalytic samples as shown in Figure 36 to study changes in the oxidation states and composition of the catalyst. Co $2p_{3/2}$ signal was observed at 782.78 eV and Co $2p_{1/2}$ signal at 798.78 eV as broad peaks with high FWHM (>4 eV) in the pristine electrode, which corresponds well with standard Co^{II} (782.28 eV and 798.38 eV respectively).[64] Additionally, scalable satellite bands were

observed 4-8 eV above the principle signals. Where in the post catalytic electrode a slight shift to lower binding energies (~2.5 eV) was observed with Co $2p_{3/2}$ signal at 780.48 eV and Co $2p_{1/2}$ at 795.88 eV.[65] The signals appear relatively sharper, with lower FWHM (~3 eV) and the satellite bands, though identifiable, are less distinctive. Earlier studies reported that these changes can be attributed to partial oxidation of the surface metal sites. FTIR studies on the pristine and post catalytic electrodes have no visible changes that can be attributed to the structural or compositional changes in the catalyst. Hence, it can be said that the partial oxidation of the surface cobalt sites is not permanent and reversible.[66]

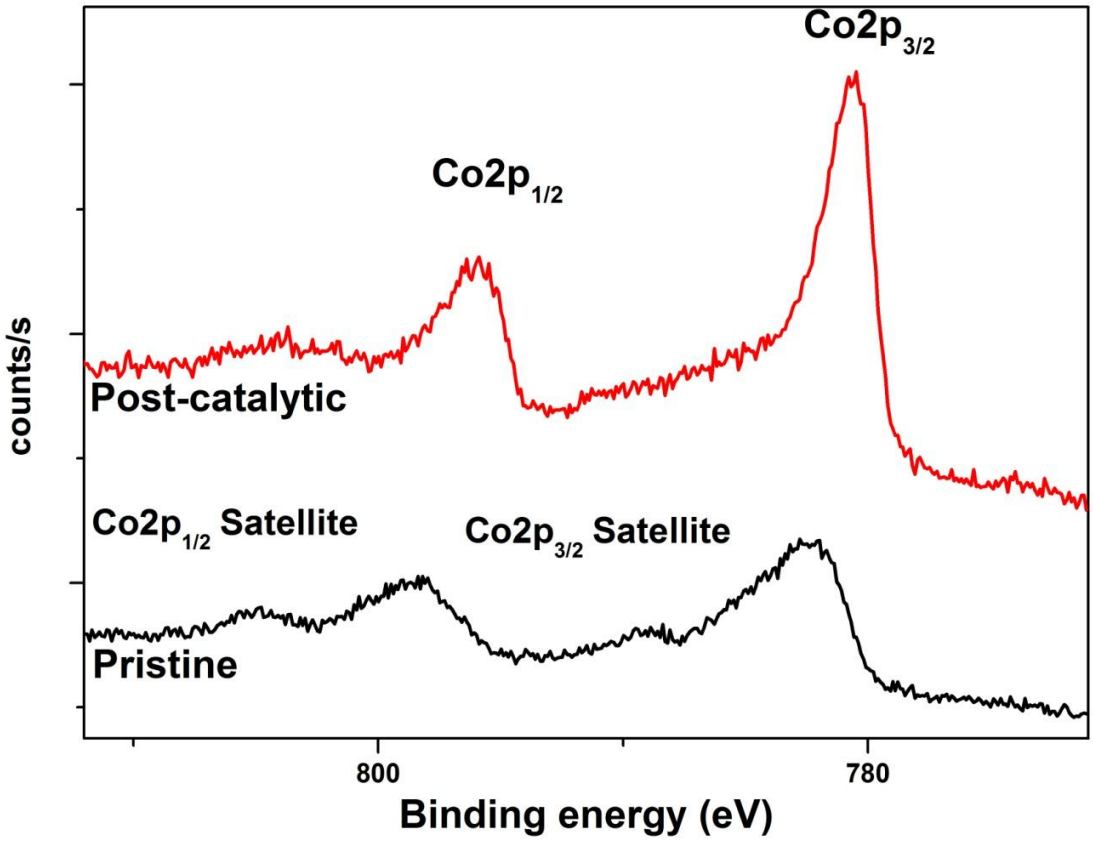

Figure 36. XPS spectra of the Co 2p region of the surface of the pristine and post-catalytic electrodes

Additionally, the O1s signal of the pristine and post catalytic samples (Figure 37) have been analyzed to study the nature of the partial oxidation. O1s signal at binding energy higher than 530 eV corresponds to oxygen species like –OH[67], adsorbed onto the surface of the catalyst, indicating the absence of any Co-O species during the course of the electrolysis.[56] The mild shift in the O1s position and the relatively higher intensity can be contributed to partial replacement of DMF on the surface with water due to their miscibility.

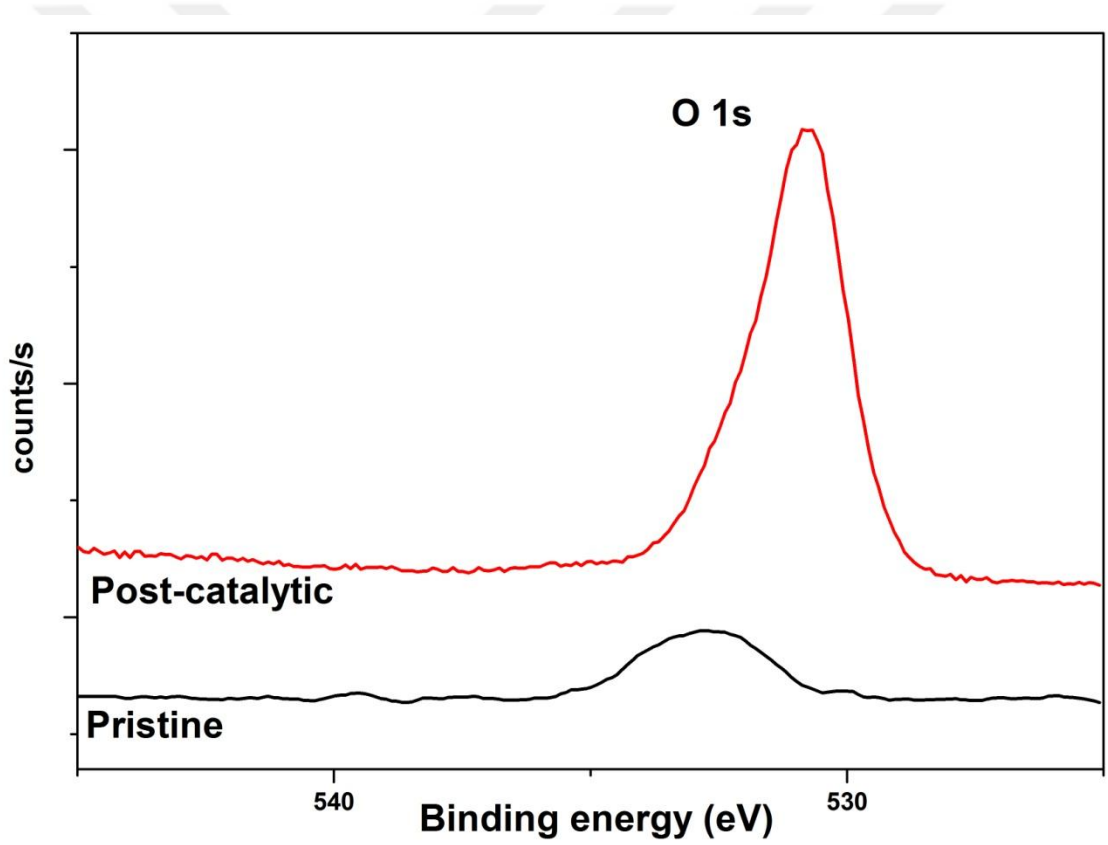

Figure 37. XPS spectra of the O 1s region of the surface of the pristine and post-catalytic electrodes

4.2. Electrochemical Studies of Metal Dicyanamides

4.2.1. Cyclic Voltammetry and Catalytic Activity Measurements of Metal Dicyanamides

Cyclic Voltammetry (CV) measurements of $Co(dca)_2(DMF)_2$, $Fe(dca)_2(DMF)_2$ and $Ni(dca)_2(DMF)_2$ were performed under nitrogen atmosphere with a scan rate of 50 mV/s between 0 V and 1.5 V (vs. Ag/AgCl) in the electrolyte of 50 mM KPi (pH 7) containing 1 M KNO_3. Although metal dicyanamides are isostructual the catalytic activity of $Co(dca)_2(DMF)_2$ is better than the other ones as shown in Figure 38.

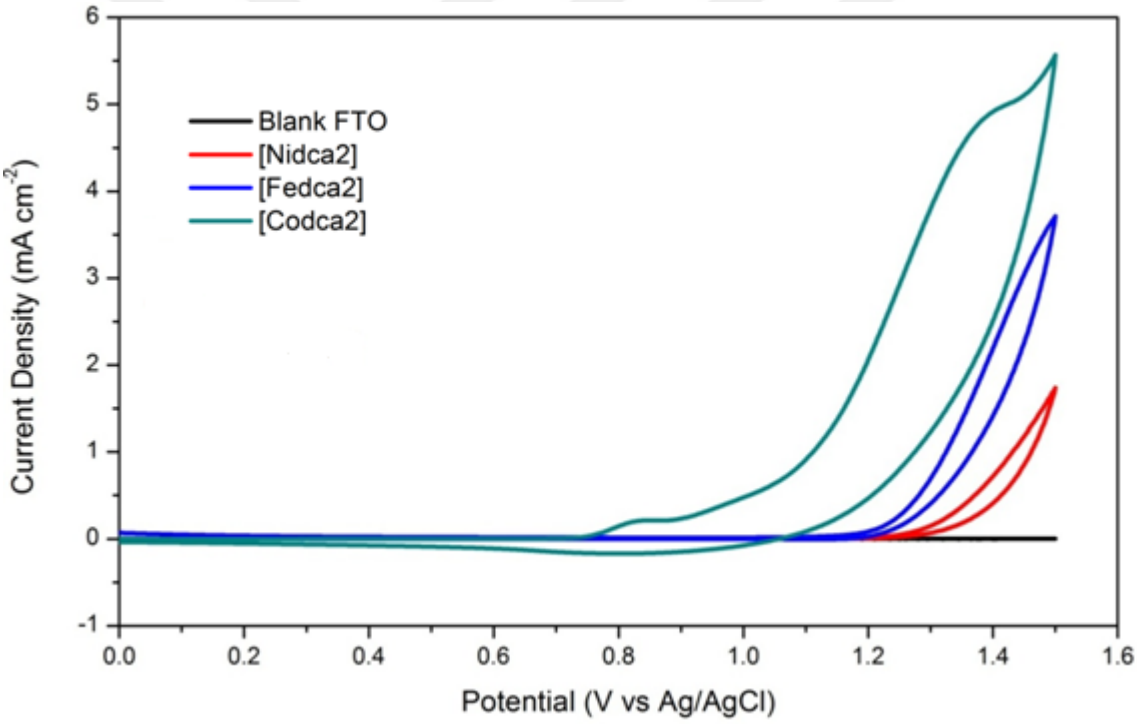

Figure 38. Cyclic voltammograms of metal dicyanamides

The following studies mainly focus on the $Co(dca)_2(DMF)_2$ due to its high catalytic performance.

Cyclic voltammograms of $Co(dca)_2(DMF)_2$ was performed in the range of 0 V-1.5 V vs. Ag/AgCl reference electrode as shown in Figure 39. It shows a quasi-reversible redox couple with a significant oxidation peak at 0.95 V and a reduction peak at 0.83 V vs. Ag/AgCl reference electrode ($E_{1/2}$ = 0.89 V, Ec − Ea = 120 mV) which can be attributed to Co^{2+}/Co^{3+} redox couple. Also, a second oxidation process was observed at 1.35 V vs. Ag/AgCl, which can be assigned to catalytic water oxidation process.[68]

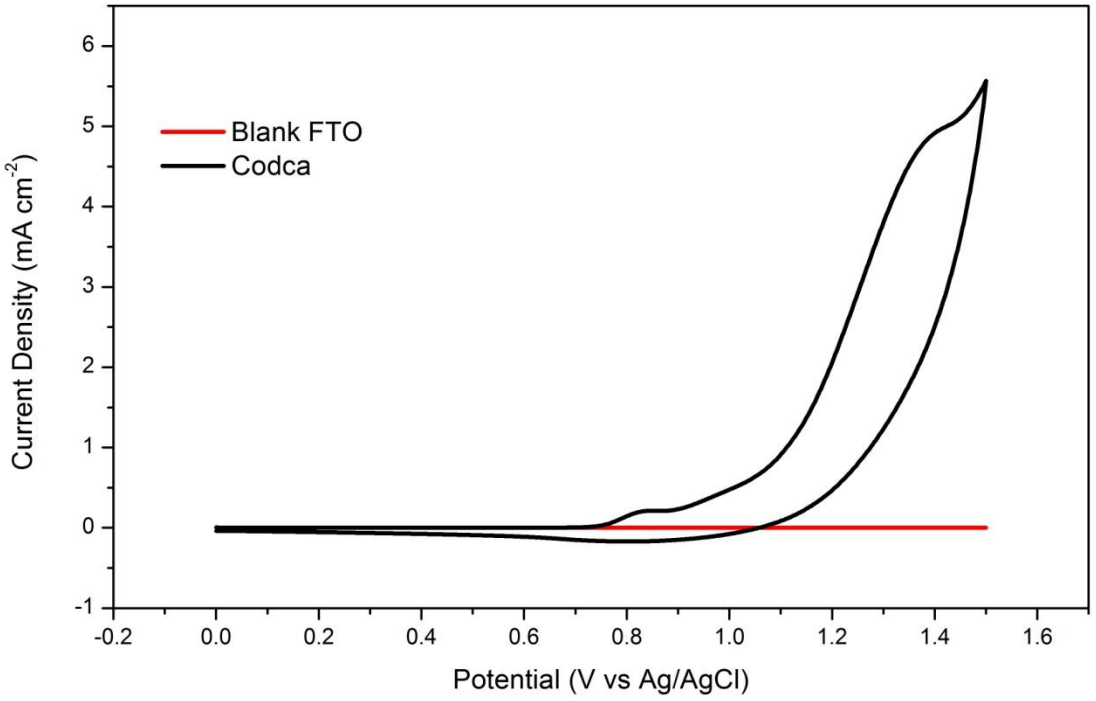

Figure 39. Cyclic voltammogram of $Co(dca)_2(DMF)_2$

For the determination of the coverage of redox-active Co centers on the electrode, cyclic voltammogram was recorded between 0.5 V - 1.1 V vs. Ag/AgCl reference electrode with different scan rates as illustrated in Figure 40.a, with the help of the slope, Figure 40.b, the concentration of the redox active center was calculated as 5.8 nmol/cm^2 by the equation 3 below.

Slope= $\frac{n^2F^2\,A\Gamma}{4RT}$ (Eq. 3)

n =1 (1 e$^-$ redox process), F= Faraday's constant, A= Surface Area,

Γ =Surface concentration (mol/cm^2), R= ideal gas constant, and T= Temperature

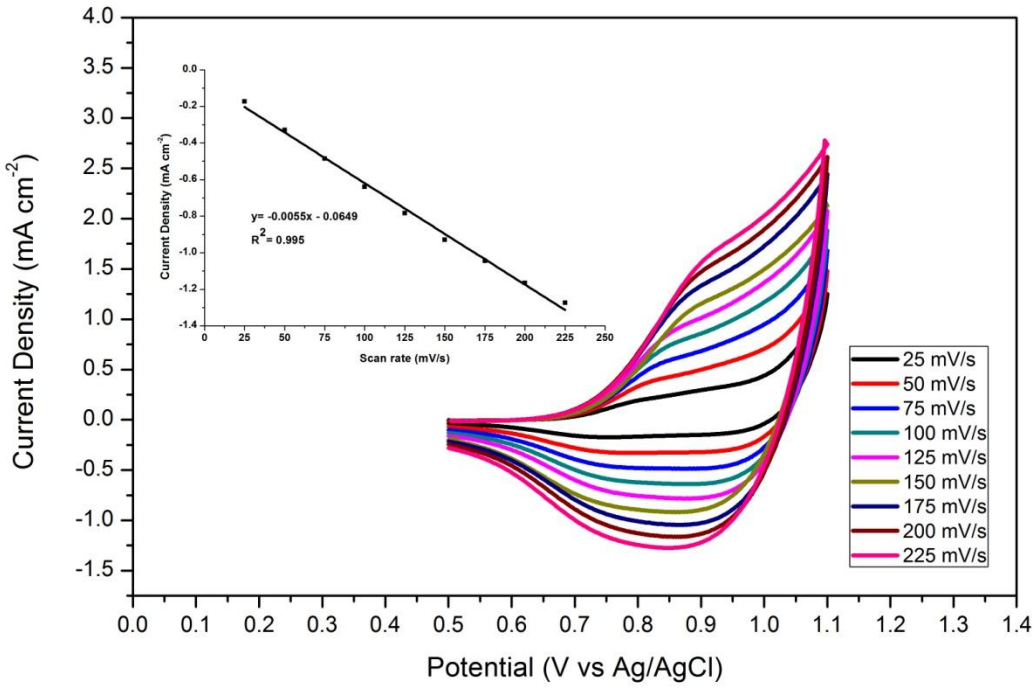

Figure 40. a) Cyclic voltammogram of $Co(dca)_2$ at different scan rate (25-225 mV sec^{-1})
b) Linear dependence of the peak current of the Co^{2+}/ Co^{3+} oxidation peak vs. scan rate.

Chronoamperometry measurements for assessment of catalytic activity of modified electrode was performed at different applied potentials in a two-compartment cell with a glass frit separation in pH 7.0 KPi buffer solution with 1 M KNO_3 as electrolyte. Steady current densities at the end of 600 sec were plotted vs. overpotential as shown in Figure 41. It shows linear behaviour between 323 - 483 mV with slope 94 mV / decade, with a current density of 1 $mAcm^{-2}$ at η= 580 mV. Surface concentration was used to determine turnover frequency (TOF) 2×10^{-3} at η= 218 mV while the TOF value = 2×10^{-3} and 2.6×10^{-3} were reported at 300 mV and 410 mV for $CoFe(CN)_6$-modified FTO electrode[51] and cobalt oxide film at pH 7.0, respectively.[69]

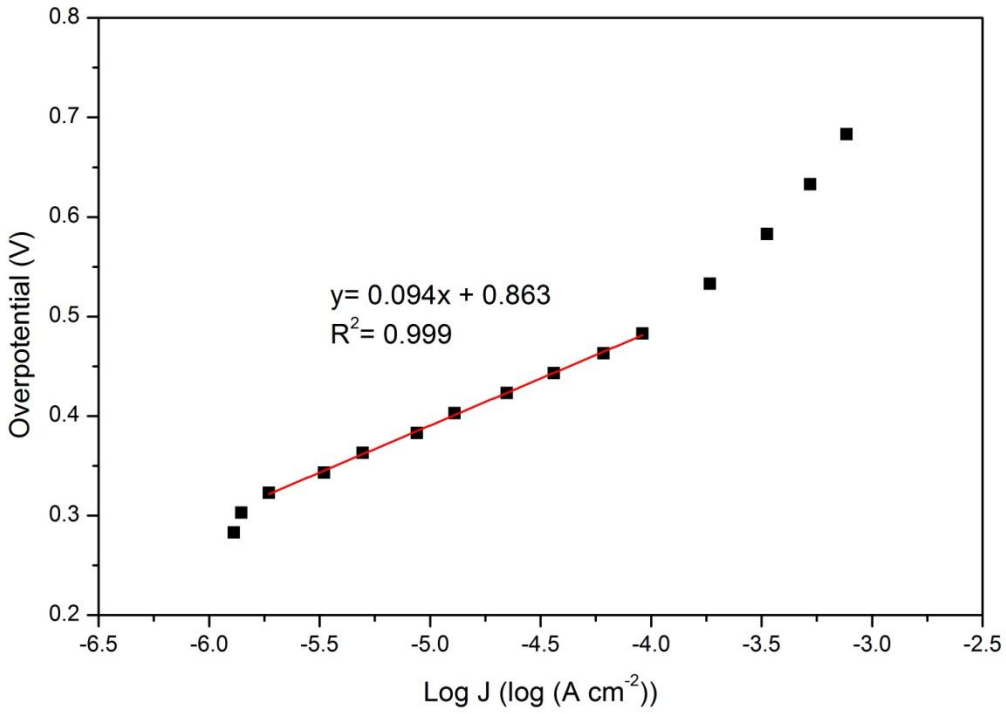

Figure 41. Tafel plots for $Co(dca)_2$ obtained in 50 mM KPi buffer solution with 1 M KNO_3 as electrolyte

To determine the stability of $Co(dca)_2$ compounds, chronoamperometry studies were performed at 1.2 V vs. Ag/AgCl for 3 days as shown in Figure 42. During this period, the experiment was realized with 12 hours intervals. In the first 12 hours interval of the experiment, the current density decreased until 2.5 hours and then started to increase for a while, lately current density decreased until reaching stabilization at almost 0.2 $mA.cm^{-2}$ after 12 h. During the other 12 hours intervals, similar current densities were observed, which indicate that cobalt dicyanamides are robust and retain their structures during the catalytic process.

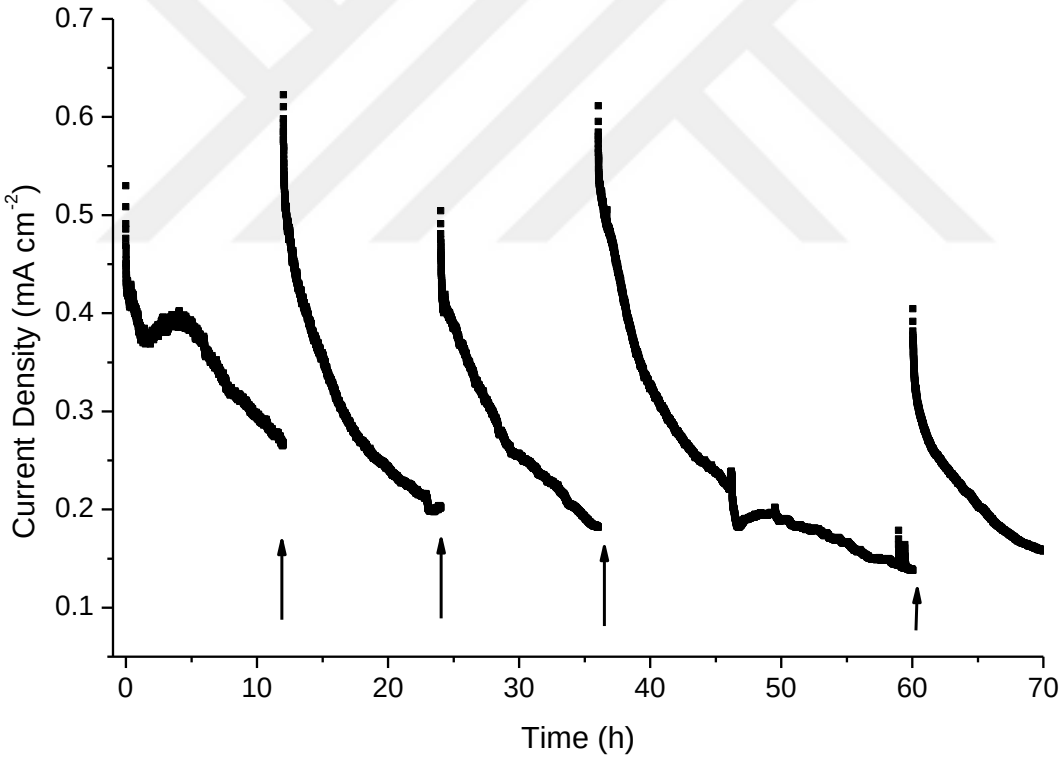

Figure 42. Long-term electrolysis profile of $Co(dca)_2$ modified electrodes for 3 days at 1.2 V vs. Ag/AgCl.

The O_2 formation was measured at 1.2 V constant potential and detected by YSI 5100 oxygen-sensing instrument equipped with a dissolved oxygen field probe inserted into the anodic compartment. The faradaic efficiency of the process is performed by bulk electrolysis for 3 hours. O_2 evolution is compared with theoretical amount calculated from Faraday's law for a $4e^-$ redox process as shown in Figure 43. The amount of dissolved O_2 molecules detected during bulk electrolysis matches the theoretical amount of evolved O_2 with an efficiency of 100%. This confirms that no competing redox reactions are taking place and that current density is quantitative for oxygen production.

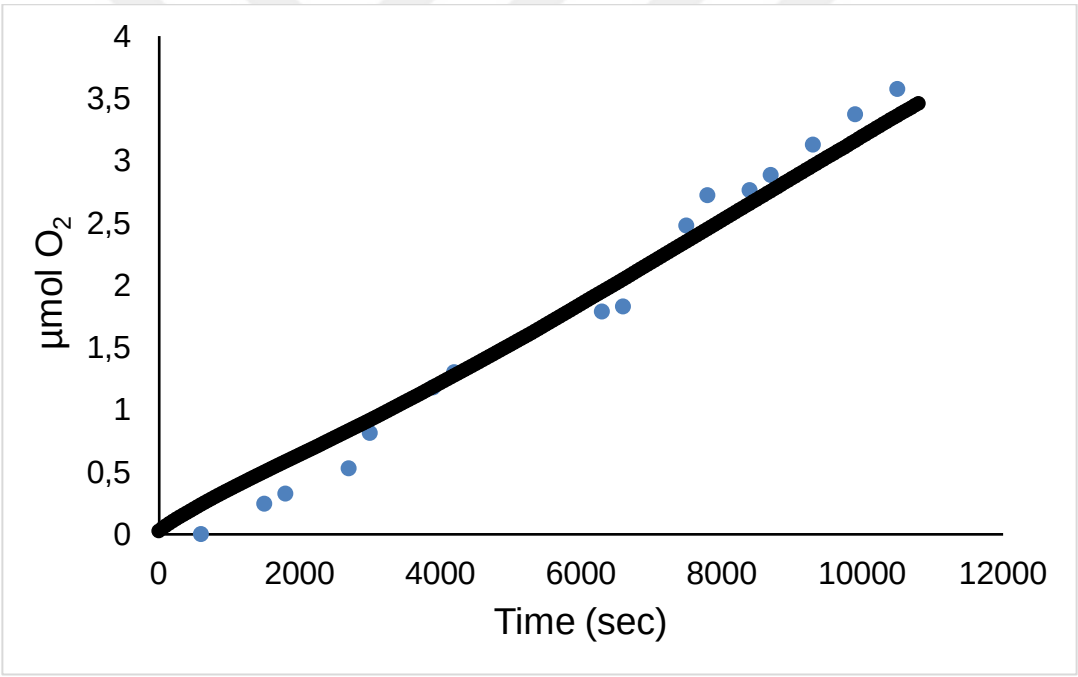

Figure 43. Catalytic oxygen evolution recorded (blue) during bulk electrolysis and theoretical assuming Faradaic behavior (black).

4.2.2. Mixed Metal Dicyanamides as WOCs

Introduction of a secondary metal ion such as Ni to cobalt based heterogeneous WOCs has been studied previously for both oxide and non-oxide systems.[70] It was shown that this method can lead to enhanced water oxidation performances. This strategy has been employed for the catalysts studied herein as well not only to obtain a detailed mapping of catalytic performances of mixed-metal dicyanamides but also to investigate the origin of the effect of doping to catalytic activity. Five different mixed metal dicyanamides, $Co_{0.5}Ni_{0.5}(dca)_2(DMF)_2$, $Co_{0.5}Fe_{0.5}(dca)_2(DMF)_2$, $Co_{0.9}Fe_{0.1}(dca)_2(DMF)_2$, $Co_{0.9}Ni_{0.1}(dca)_2(DMF)_2$, and $Co_{0.9}Ni_{0.05}Fe_{0.05}(dca)_2(DMF)_2$ with different stoichiometric ratios of Co, Fe, and Ni were synthesized using the same synthesis protocols in addition to three compounds $M(dca)_2(DMF)_2$ (Co, Ni, and Fe). The increase in the catalytic activity was determined with partial Ni substitution of Co sites in $Co(dca)_2$ system. To determine the structural, morphological, and compositional effect of Ni in the compound, they were characterized with XRD, FT-IR, SEM, EDX, and XPS.

The XRD patterns of compounds and their infrared spectra are shown in Figures 44 and 45, which indicate that compounds are isostructural. Low degrees of crystallinities particularly for Fe derivatives were obtained due to their hygroscopic nature.

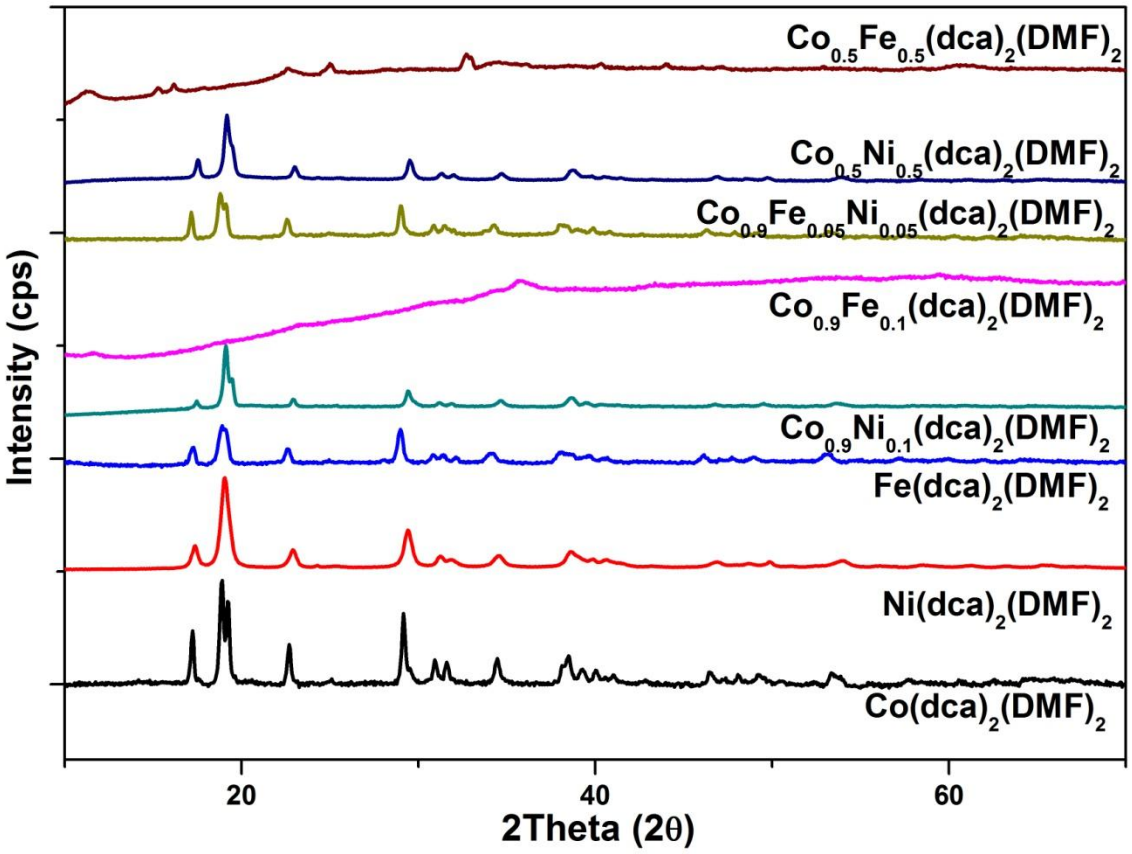

Figure 44. XRD patterns of metal dicyanamide compounds.

Applying Scherrer formula, crystallite sizes of these compounds were calculated, which reveal a phenomenal change. The crystallite sizes dropped down to 602 Å and 584 Å, respectively, in $Co_{0.9}Ni_{0.1}(dca)_2(DMF)_2$ and $Co_{0.5}Ni_{0.5}(dca)_2(DMF)_2$, compared to $Co(dca)_2$.

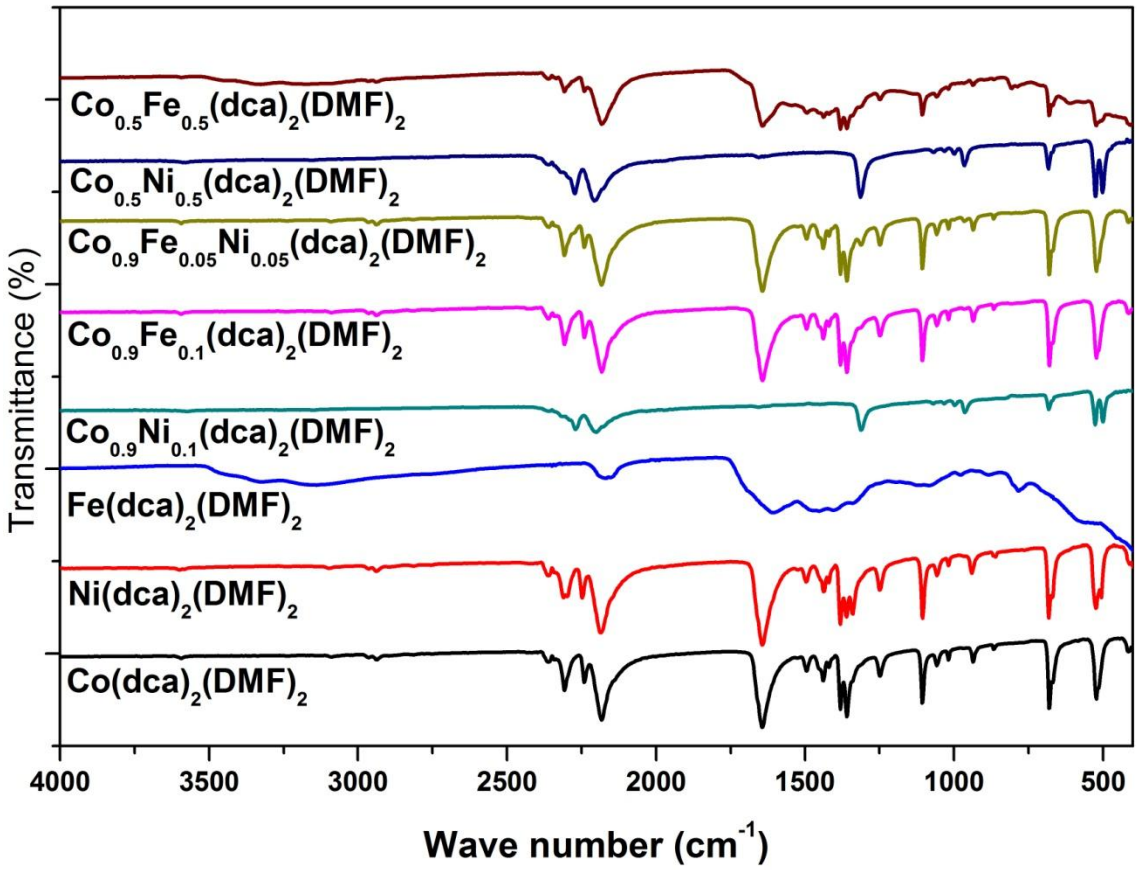

Figure 45. FTIR spectra of metal dicyanamide compounds

In the wavenumber ranges of 2360 – 2184 cm^{-1} $\nu_{sym\&asym(C\equiv N)}$ stretching, around 1380 – 1364 cm^{-1} ν_{asym}(C-N), and at around 938 cm^{-1} ν_{sym}(C-N), which can be attributed to the cyanide group in dicyanamide group.[59] Strong bands in the wavenumber range of 1108 – 1015 cm^{-1} corresponding to C-N group, bands at around 1647 – 1640 cm^{-1} can be assigned to the (C=O) stretches, and bands at around 2970 – 2934 cm^{-1} can be assigned to aliphatic ν(C-H) stretching vibrations of DMF.[63] In the Fe compound, there is broad stretching at around 3500 – 3250 cm^{-1} and the reason can be because of the excess moisture adsorbed.

The SEM images obtained for the compounds displayed in Figure 46 show a significant change in the morphology of the particles with the addition of nickel. Even though there is no noticable change in the crystalline structures of $Co(dca)_2(DMF)_2$ and $Co_{0.9}Ni_{0.1}(dca)_2(DMF)_2$ (Figure 44.); the apparent change in the morphology of particles from agglomerated compound to well defined needle-like forms can be contributed to the change in the composition which may have resulted in little change in the surface charges of the catalyst.

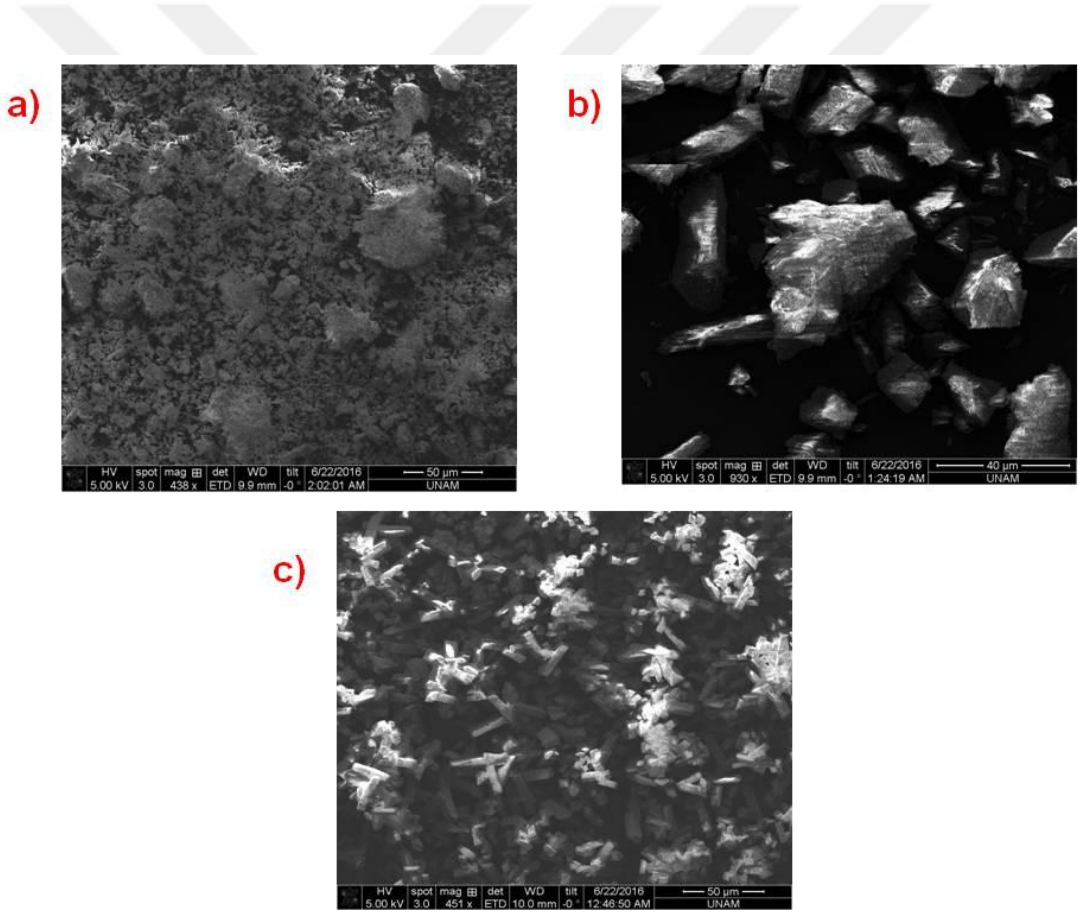

Figure 46. SEM images of a) $Co(dca)_2(DMF)_2$, b) $Co_{0.9}Ni_{0.1}(dca)_2(DMF)_2$, and c) $Co_{0.5}Ni_{0.5}(dca)_2(DMF)_2$

Nitrogen sorption measurements of $Co(dca)_2$ and mix Co/Ni $(dca)_2$ catalysts were realized to deduce the surface area. Initially, the samples were subjected to N_2-sorption measurements by studying the N_2 adsorption and desorption isotherms at 77 K as illustrated in Figure 47. All of the samples appear to exhibit porous behavior with varying surface areas. $Co(dca)_2$ appears to have the least surface area whereas $Co_{0.5}Ni_{0.5}(dca)_2(DMF)_2$ exhibits relatively higher surface area with more uniform porosity, which corresponds well with the crystallite size calculations made from XRD results and morphological changes observed in SEM imaging (Table 7).

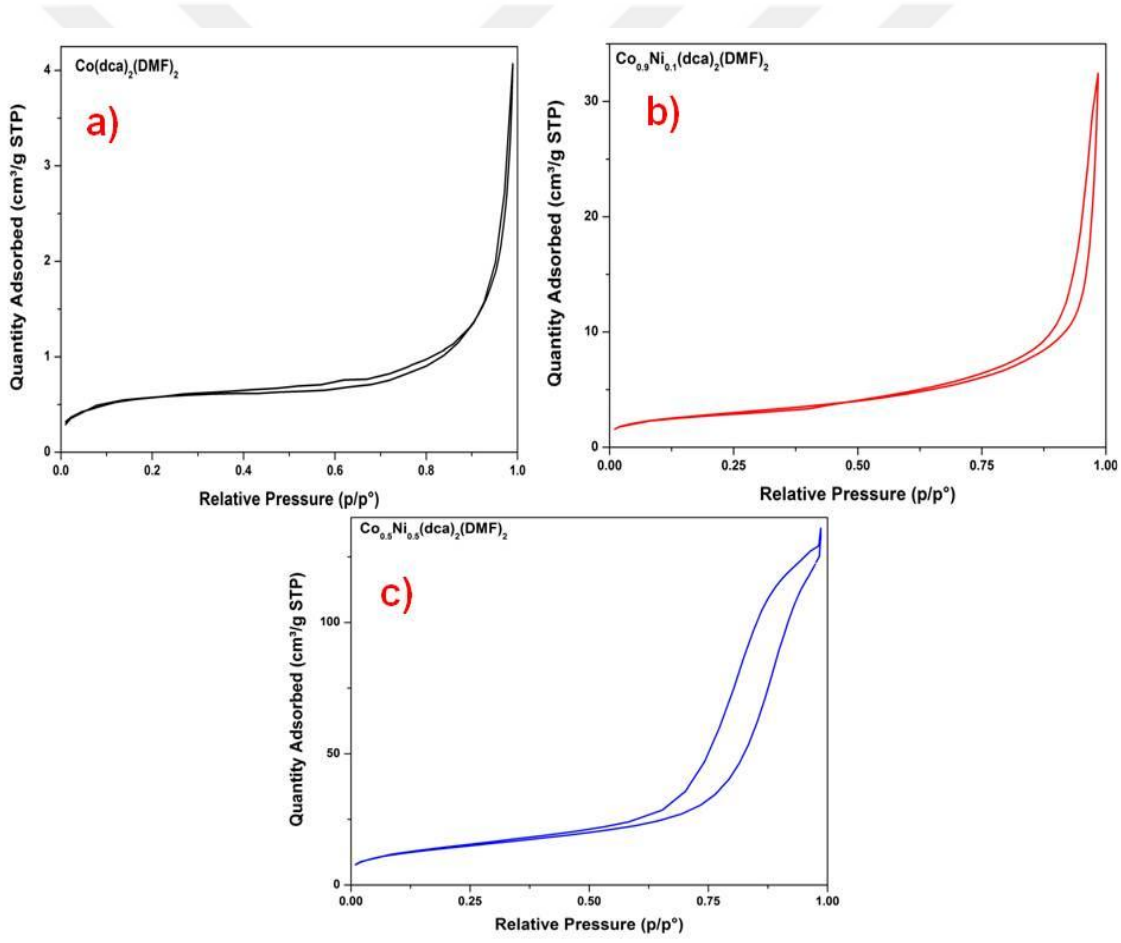

Figure 47. N_2 sorption isotherms of a) $Co(dca)_2(DMF)_2$, b) $Co_{0.9}Ni_{0.1}(dca)_2(DMF)_2$, and c) $Co_{0.5}Ni_{0.5}(dca)_2(DMF)_2$.

Table 7. The structural and elemental composition representation of the compounds

$M(dca)_2(DMF)_2$	**EDX**	**Surface Concentration (nmol*cm^{-2})**	**S_{BET} (m2/g)**	**Pore size (Å)**	**Crystallite size (Å)**
Fe	-	-	-	-	580
Ni	-	-	-	-	205
Co	-	5.8	2.0	98.9-298.79	>1000
$Co_{0.9}Ni_{0.1}$	9.098 : 0.902	6.3	10.2	157.525 - 230.178	602
$Co_{0.5}Ni_{0.5}$	1.02 : 0.98	5.0	50.9	110.392 – 166.27	584

The compositions of these compounds were confirmed by EDX analysis.

An increase in the current density was observed upon replacement of Co with Ni and maximum performance was observed for $Co_{0.5}Ni_{0.5}dca_2$ (Figure 48). Although the pristine catalyst $Ni(dca)_2$ had relatively very low activity for water oxidation, partial substitution of Co with Ni atoms in $Co(dca)_2$ resulted in higher water oxidation activity due to change in the morphology of the matrix and, thus, increase in the availability of electroactive Co centers on the surface.

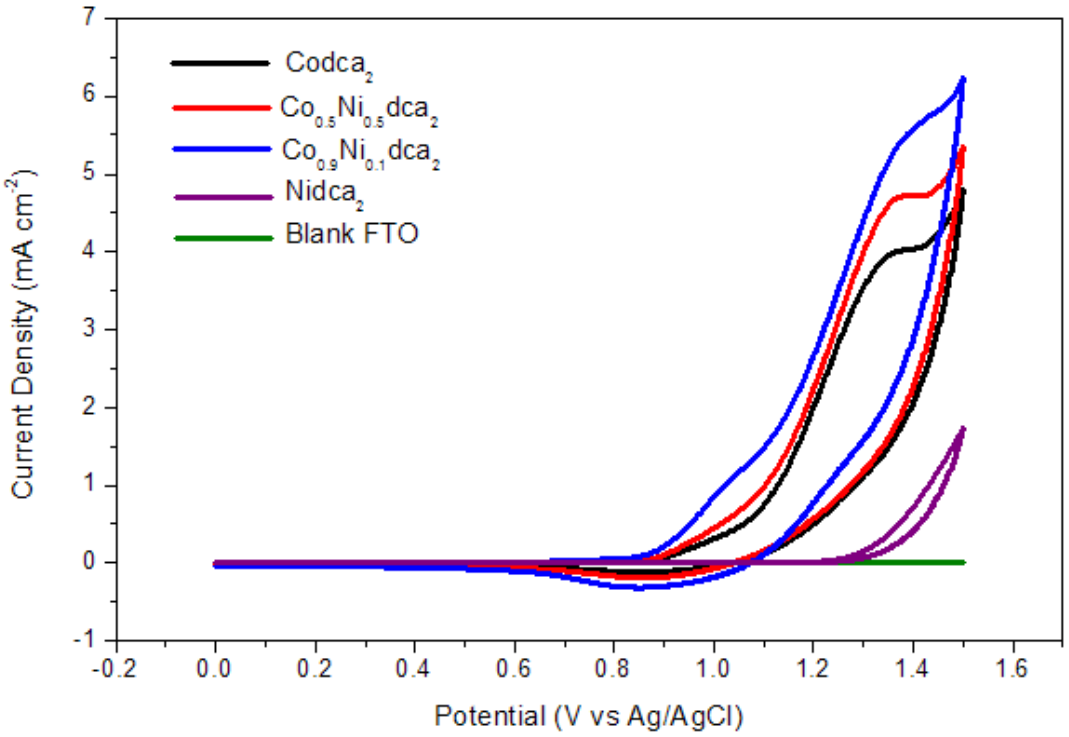

Figure 48. Cylic voltammograms of the $Co(dca)_2$, $Ni(dca)_2$, and $Co_{1-x}Ni_x(dca)_2$ (x = 0.1 & 0.5) recorded in 50 mM KPi buffer solution with 1 M KNO_3 as electrolyte at pH = 7.0 with a sweep rate of 50 mV/s.

To determine and compare the catalytic activity of the modified electrodes, chronoamperometry measurements were performed at different applied potentials in KPi buffer solution with 1 M KNO_3 at pH 7.0. Steady current densities at the end of 600 sec. were plotted versus overpotential as shown in Figure 49.

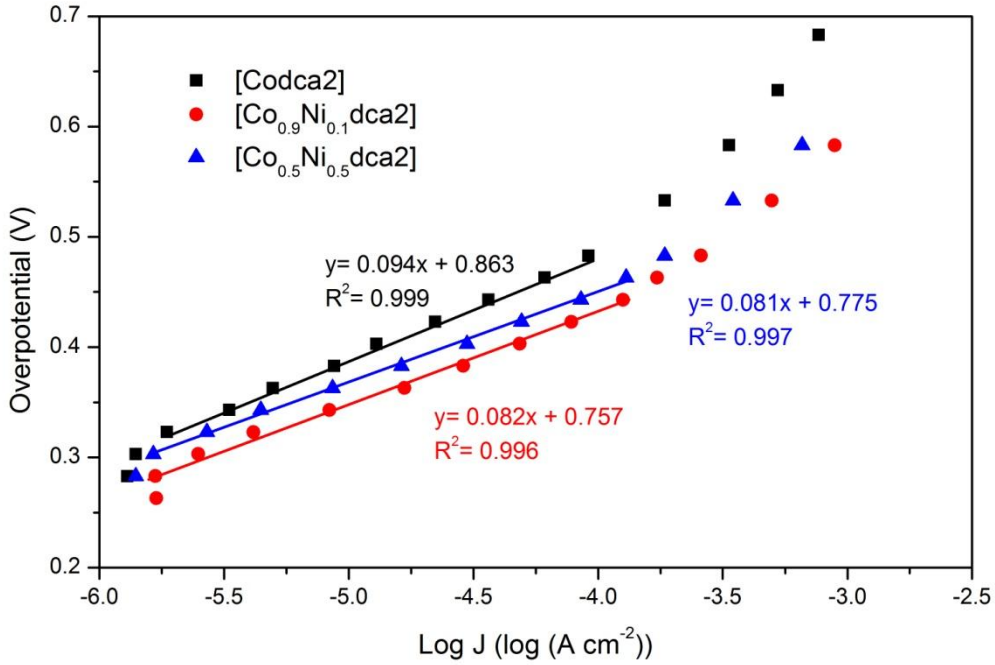

Figure 49. Tafel plots obtained for $Co(dca)_2$, $Co_{0.9}Ni_{0.1}(dca)_2$, and $Co_{0.5}Ni_{0.5}(dca)_2$.

The catalytic parameters of the $Co(dca)_2$, $Co_{0.9}Ni_{0.1}(dca)_2$ and $Co_{0.5}Ni_{0.5}(dca)_2$ were summarized and compared to other compounds in Table 8.

Table 8. The catalytic representation of the compounds

Compound	**η,onset overpot. (mV)**	**$\eta^{(b)}$ overpot. (mV)**	**Tafelslope (mV decade^{-1})**	**pH**	**TOF (s^{-1})**	**Surface concentration (nmol*cm^{-2})**
CoFePBA[53]	291	>600	88	7	2×10^{-3} (η= 300)	
CoPOM/MCN[71]	380	-	230	7	0.3 (η= 780)	
$Codca_2$	323	580	94	7	2×10^{-3} (η= 356)	5.8
$Co_{0.9}Ni_{0.1}dca_2$	283	513	82	7	2×10^{-3} (η= 324)	6.3
$Co_{0.5}Ni_{0.5}dca_2$	303	531	81	7	2×10^{-3} (η= 334)	5.0

As shown in Table 8, Ni substitution increases the catalytic activity and makes the compounds comparable to other compounds.

The current densities of the $Co(dca)_2$, $Fe(dca)_2$, $Ni(dca)_2$, $Co_{0.5}Ni_{0.5}(dca)_2$, $Co_{0.9}Ni_{0.1}(dca)_2$, $Co_{0.5}Fe_{0.5}(dca)_2$, $Co_{0.9}Fe_{0.1}(dca)_2$, and $Co_{0.9}Fe_{0.05}Ni_{0.05}(dca)_2$ compounds were measured at the end of the 600 sec under 1.2 V applied potentials to show the catalytic performance. The comparisons of the each compound were shown in Figure 50. The contour plot show the higher current density, when nickel concentration is 10-50% for the binary compounds and lower current density with the increase of the Fe amount in the compounds.

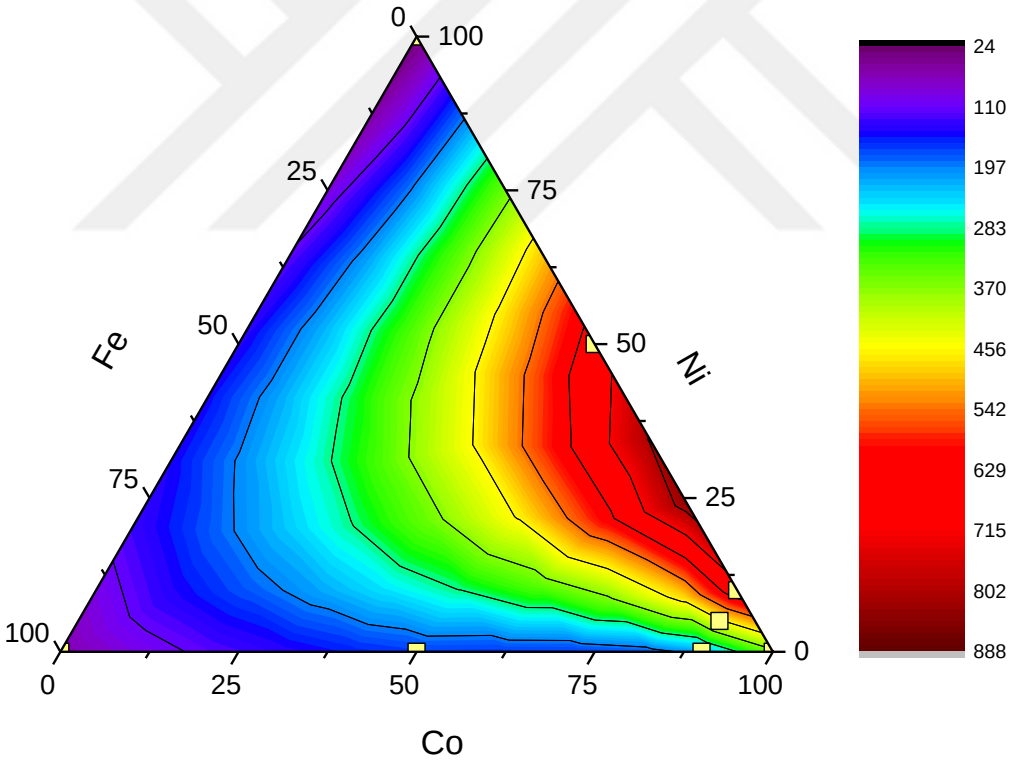

Figure 50. Contour plot of the mixed metal dicyanamides obtained by chronoamperometric studies at 1.2 V (vs. Ag/AgCl electrode) for 600 sec.

Chapter 5

CONCLUSION

In this thesis, a new metal dicyanamide compound $Co(hmt)(dca)_2$ was synthesized, characterized, and studied for its potential application in the field of selective CO_2/N_2 separation. The network consists of octahedral Co(II) metal center, as well as hmt and dicyanamide groups coordinated to the metal center. In the compound, one free nitrogen atom that belongs to dicyanamide and two free nitrogen atoms that belong to hmt groups are available. The availability of the free nitrogen atoms inside the pores increases the selective adsorption of CO_2 due to Lewis acidic behavior of CO_2. In the $Co(hmt)(dca)_2$ crystal, the pore opening is almost 3.8 Å while kinetic diameters of N_2 and CO_2 are 3.6 Å and 3.3 Å, respectively. The similarity between kinetic diameter of the crystal and N_2 results in limited diffusion of N_2, which is believed to be the origin of the high selectivity obtained in this study.

Metal dicyanamides have also been investigated as water oxidation catalysts in this thesis. This is the first study that investigates the catalytic properties of metal dicyanamides. Simple metal dicyanamides without coligands, $M(dca)_2$, were used in this part of thesis. A new family of metal dicyanamides, $M(dca)_2(DMF)_2$ (M = Fe, Co, Ni), were obtained and characterized in detail by X-ray diffraction and infrared spectroscopy. Electrochemical studies showed that Co derivative exhibited the highest catalytic activity as expected. Further electrocatalytic studies performed on Co derivative indicate that a current density of 1 $mA.cm^{-2}$ could be obtained at an overpotential of 580 mV and this value could be decreased down to 513 mV with Ni doping. A turnover frequency of

2×10^{-3} h^{-1} could be obtained at η = 356, 324, 334 for $Co(dca)_2(DMF)_2$, $Co_{0.9}Ni_{0.1}(dca)_2(DMF)_2$, and $Co_{0.5}Ni_{0.5}(dca)_2(DMF)_2$, respectively.

All in all, the study showed that the rich and diverse chemistry of metal dicyanamides could have potential applications in gas separation and catalytic application thanks to their porous nature and metal content. The fact that their synthetic protocol is flexible and that it enables easy tuning of structures can be used to establish correlations between structure and application.

BIBLIOGRAPHY

1. Jun, L., Lijuan, Q., Baoshu, L., Xinrong,Z., Feng, Y. and Lili, C. Synthesis, Structure and Magnetic Properties of Two Cobalt(II) Dicyanamide (dca) Complexes with Heterocyclic Nitrogen Donors Tetra(2-pyridyl)pyrazine (tppz) and 2,4,6-Tri(2-pyridyl)-1,3,5-triazine (tptz): $[Co_2(tppz)(dca)_4]\cdot CH_3CN$ and [Co(tptz)(dca)(H2O)]. *Chinese J. Chem.* **30,** 522–528 (2012).
2. Werf, P., Batten, S., Jensen, P., Moubaraki, B., Murray, K. and Cashion, J. Structure and Magnetism of 3D Anionic Metal Dicyanamide $(Me_3Ph_3P)[M(dca)_3]$ (M= Fe, Co, Ni) and $(EtPh_3P)$ $[M(dca)_3]$ (M=Mn, Co, Ni) Networks. *Cyrstal Growth & Design*, **4**, 503-508 (2004).
3. Zheng, L.-L. and Zhuang, X.-M. Syntheses, Crystal Structures and Magnetism of Three Metal-Dicyanamide Coordination Polymers with Isonicotinamide Co-Ligand. *Zeitschrift für Anorg. und Allg. Chemie* **636,** 2500–2507 (2010).
4. Köhler, H. Beitrage zur Chemie des Dicyanamid- und des Tricyanmethanidions. I. Die Bildung von Übergangsmetall-Pyridin-Komplexen. *Zeitschrift für Anorg. und Allg. Chemie* **331,** 237–248 (1964).
5. Köhler, H. and Seifert, B. Beiträge zur Chemie des Dicyanamid- und des Tricyanmethanid-Ions. IV. Kobalt(II)-dicyanamid-und -tricyanmethanid-Komplexe. *Zeitschrift für Anorg. und Allg. Chemie* **344,** 63–71 (1966).
6. Manson, J. L. in *Magnetism: Molecules to Materials V* 71–104 (Wiley-VCH Verlag GmbH & Co. KGaA, 2004).

7. Noro, S. I., Kitaura,R., Kondo, M., Kitagawa, S., Ishi, T., Matsuzaka, H. and Yamashita, M. Framework engineering by anions and porous functionalities of Cu(II)/4,4′-bpy coordination polymers. *J. Am. Chem. Soc.* **124,** 2568–2583 (2002).

8. Wu, G., Bai, J. and Jiang, Y. Rolling Up the sheet: Constructing metal-organic lamellae and nanotubes from a [{mn_3(propanediolato)$_2$}(dicyanamide) $_2$]n honeycomb skeleton. *J. Am. Chem. Soc.* **135,** 18276–18279 (2013).

9. Batten, S. R., Jensen, P., Moubaraki, B., Murray, K. S. and Robson, R. Structure and molecular magnetism of the rutile-related compounds M(dca)$_2$, where M = CoII, NiII, CuII, dca = dicyanamide, $N(CN)_2^-$. *Chem. Commun.* 439–440 (1998).

10. Batten, S. R. and Murray, K. S. Structure and magnetism of coordination polymers containing dicyanamide and tricyanomethanide. *Coord. Chem. Rev.* **246,** 103–130 (2003).

11. Manna, S. C., Ghosh, A. K., Ribas, J., Drew, M., Lin, C., Zangrando, E. and Chaudhuri N.R. Synthesis, crystal structure, magnetic behavior and thermal property of three polynuclear complexes: $[M(dca)_2(H2O)_2]_n\cdot(hmt)_n$ [M = Mn(II), Co(II)] and $[Co(dca)_2(bpds)]_n$ [dca, dicyanamide; hmt, hexamethylenetetramine; bpds, 4,4′-bipyridyl disulfide]. *Inorganica Chim. Acta* **359,** 1395–1403 (2006).

12. Kohout, J., Jäger, L., Hvastijová, M. and Kožíšek, J. Tricyanomethanide and Dicyanamide Complexes of Cu(II), Ni(II), Co(II), Their Structures and Properties. *J. Coord. Chem.* **51,** 169–218 (2000).

13. Kurmoo, M. and Kepert, C. J. Hard magnets based on transition metal complexes with the dicyanamide anion,{$N(CN)_2$}. *New J. Chem.* 1515–1524 (1998).

14. Kmety, C., Manson, J. and McCall, S. Low-temperature specific heat of the molecule-based magnet $M[N(CN)_2]_2$ (M=Co, Ni, Cu, Zn) series. *J. Magn. Magn. Mater.* **248,** 52–61 (2002).

15. Armentano, D., De Munno, G., Guerra, F., Julve, M. and Lloret, F. Ligand effects on the structures of extended networks of dicyanamide-containing transition-metal ions. *Inorg. Chem.* **45,** 4626–4636 (2006).

16. Batten, S., Jensen, P. and Kepert, C. Syntheses, structures and magnetism of α-$Mn(dca)_2$, $[Mn(dca)_2(H_2O)_2]\cdot H_2O$, $[Mn(dca)_2(C_2H_5OH)_2]\cdot(CH_3)_2CO$, $[Fe(dca)_2(CH_3OH)_2]$ and $[Mn(dca)_2(L)_2]$, where L = pyridine, CH_3OH or DMF and dca= dicyanamide, N(CN)2. *J. Chem. Soc., Dalt. Trans.* **22,** 2987–2997 (1999).

17. Kmety, C., Manson, J., Huang, Q., Lynn, J., Erwin, R., Miller, J. and Epstein, A. Collinear ferromagnetism and spin orientation in the molecule-based magnets $M[N(CN)_2]_2$ (M=Co,Ni). *Phys. Rev. B* **60,** 60–63 (1999).

18. Luo, J., Hong, M., Cao, R., Liang, Y., Zhao, Y., Wang, R. and Weng, J. Syntheses and crystal structures of cadmium (II) coordination polymers with end-to-end dicyanamide bridges. **21,** 1–6 (2002).

19. Dalai, S., Sarathi Mukherjee, P., Zangrando, E. and Ray Chaudhuri, N. Synthesis, crystal structure and magnetic properties of two new dicyanamide bridged 2D and 1D complexes of Mn(ii). *New J. Chem.* **26,** 1185–1189 (2002).

20. Wang, Z., Sun, B. and Luo, J. Bimetallic sheet and 3D threefold interpenetrating diamond-like network constructed by chelate Cu cations and Mn dicyanamide polymeric chains. Synthesis, crystal structure, and magnetism of

[$Cu(L)_2$][$Mn(dca)_4$] . *Inorganica Chim. Acta* **332,** 127–134 (2002).

21. Jensen, P., Batten, S. R., Moubaraki, B. and Murray, K. S. Syntheses, crystal structures, and magnetic properties of first row transition metal coordination polymers containing dicyanamide and 4,4′-bipyridine. *J. Chem. Soc. Dalt. Trans.* **1,** 3712–3722 (2002).

22. Van der Werff, P. M., Batten, S. R., Jensen, P., Moubaraki, B. and Murray, K. S. Cation Templation of Anionic Metal Dicyanamide Networks. *Inorg. Chem.* **40,** 1718–1722 (2001).

23. Raebiger, J. W., Manson, J. L., Sommer, R. D., Geiser, U., Rheingold, A.L. and Miller, J. S. 1-D and 2-D Homoleptic Dicyanamide Structures , $[Ph_4P]_2\{ Co^{II}[N(CN)_2]_4\}$ and $[Ph_4P]_2\{ M[N(CN)_2]_3\}$ (M=Mn, Co). *Inorg. Chem.* **40,** 2578–2581 (2001).

24. Tabrizi, L., Chiniforoshan, H., McArdle, P., Tavakol, H., Rezaei, B. and Dehcheshmeh, M. M. Selective gas sorption and electrochemical properties of a dicyanamide coordination polymer: Insight from experimental and theoretical study. *Polyhedron* **69,** 84–89 (2014).

25. Ghosh, A. K., Ghoshal, D., Drew, M. G. B., Mostafa, G. and Ray Chaudhuri, N. Syntheses and crystal structures of two new coordination polymers of Cd(II) using organic spacer and inorganic-bridging ligands. *Struct. Chem.* **17,** 85–90 (2006).

26. Goldemberg, J. Energy needs in developing countries and sustainability. *Science* **269,** 1058–9 (1995).

27. Lewis, N. S. and Nocera, D. G. Powering the planet: Chemical challenges in solar energy utilization. *Proc. Natl. Acad. Sci.* **103,** 15729–15735 (2006).

28. Hoel, M. & Kverndokk, S. Depletion of fossil fuels and the impacts of global warming. *Resour. Energy Econ.* **18,** 115–136 (1996).

29. Höök, M. and Tang, X. Depletion of fossil fuels and anthropogenic climate change—A review. *Energy Policy* **52,** 797–809 (2013).

30. Hoffert, M., Caldeira, K. and Jain, A. Energy implications of future stabilization of atmospheric CO_2 content. *Nature* **395,** 881–884 (1998).

31. Jain, A. K., Kheshgi, H. S., Hoffert, M. I. and Wuebbles, D. J. Distribution of radiocarbon as a test of global carbon cycle models. *Global Biogeochem. Cycles* **9,** 153–166 (1995).

32. Schneider, S. H. and Goulder, L. H. Achieving low-cost emissions targets. *Nature* **389,** 13–14 (1997).

33. Withagen, C. Pollution and exhaustibility of fossil fuels. *Resour. Energy Econ.* **16,** 235–242 (1994).

34. Chu, S. and Majumdar, A. Opportunities and challenges for a sustainable energy future. *Nature* **488,** 294–303 (2012).

35. Service, R. F. Choosing a CO_2 Separation Technology. *Science* **305,** 963– (2004).

36. Solomon, S., Plattner, G.-K., Knutti, R. and Friedlingstein, P. Irreversible climate change due to carbon dioxide emissions. *Proc. Natl. Acad. Sci. U. S. A.* **106,** 1704–9 (2009).

37. Duan, J., Yang, Z. and Bai, J. Highly selective CO_2 capture of an agw-type metal–organic framework with inserted amides: experimental and theoretical

studies. *Chem. Commun.* **48,** 3058 (2012).

38. Bae, Y.-S., Farha, O. K., Hupp, J. T. and Snurr, R. Q. Enhancement of CO_2/N_2 selectivity in a metal-organic framework by cavity modification. *J. Mater. Chem.* **19,** 2131 (2009).

39. Bloch, W. M., Babarao, R., Hill, M. R., Doonan, C. J. and Sumby, C. J. Post-synthetic structural processing in a Metal-organic Framework material as a mechanism for exceptional CO_2 / N_2 selectivity Post-synthetic structural processing in a Metal-organic Framework material as a mechanism for exceptional CO_2 / N_2 selectivity. (2013).

40. Zheng, B., Yang, Z., Bai, J., Li, Y. and Li, S. High and selective CO_2 capture by two mesoporous acylamide-functionalized rht-type metal–organic frameworks. *Chem. Commun.* **48,** 7025 (2012).

41. Li, J., Shi, Y., Dinov, I. D. and Toga, A. W. in Multimodal Brain Image Analysis: Third International Workshop, MBIA 2013, Held in Conjunction with MICCAI 2013, Nagoya, Japan, Proceedings (eds. Shen, L. et al.) 1–8 (Springer International Publishing, 2013).

42. Srivastava, R., Srinivas, D. and Ratnasamy, P. Sites for CO_2 activation over amine-functionalized mesoporous Ti(Al)-SBA-15 catalysts. *Microporous Mesoporous Mater.* **90,** 314–326 (2006).

43. Du, L., Lu, Z., Zheng, K., Wang, J., Zheng, X., Pan, Y., You, X. and Bai, J. Fine-tuning pore size by shifting coordination sites of ligands and surface polarization of metal-organic frameworks to sharply enhance the selectivity for CO_2. *J. Am. Chem. Soc.* **135,** 562–565 (2013).

44. Escuer, A., Mautner, F. A. and Graz, A. Two New One-Dimensional Compounds with End-to-End Dicyanamide as a Bridging Ligand: Syntheses and Structural Characterization of trans - [Mn (4-bzpy) $_2$ (N(CN)$_2$) $_2$] n and cis - [Mn (Bpy) (N(CN)$_2$)$_2$] n , (4-bzpy) 4-benzoylpyridine; bp. *Inorg. Chem.* **2,** 1668–1673 (2000).

45. Nocera, D. G. The Artificial Leaf. *Acc. Chem. Res.* **45,** 767–776 (2012).

46. Ferreira, K. N., Iverson, T. M., Maghlaoui, K., Barber, J. and Iwata, S. Architecture of the photosynthetic oxygen-evolving center. *Science* **303,** 1831–8 (2004).

47. Ananyev, G. ., Zaltsman, L., Vasko, C. and Dismukes, G. . The inorganic biochemistry of photosynthetic oxygen evolution/water oxidation. *Biochim. Biophys. Acta - Bioenerg.* **1503,** 52–68 (2001).

48. Smith, P., Hunt, L. and Laursen A. Water Oxidation by the $[Co_4O_4(OAc)_4(py)_4]^+$ Cubium is Initiated by OH– Addition. *J. Am. Chem. Soc.* **137,** 15460–15468 (2015).

49. Barber, J. Photosynthetic energy conversion: natural and artificial. *Chem. Soc. Rev*. **38,** 185–196 (2009).

50. Wang, W., Wang, Z. and Zhuu, Q. Direct electron transfer from photosystem II to hematite in a hybrid photoelectrochemical cell. *Chem. Commun.* **51,** 16952–16955 (2015).

51. Pintado, S., Goberna-Ferrón, S., Escudero-Adán, E. C. and Galán-Mascarós, J. R. Fast and Persistent Electrocatalytic Water Oxidation by Co–Fe Prussian Blue

Coordination Polymers. *J. Am. Chem. Soc.* **135,** 13270–13273 (2013).

52. Kanan, M. W. and Nocera, D. G. In Situ Formation of an Water Containing Phosphate and Co 2^{+}. *Science* **321,** 1072–1075 (2008).

53. Goberna, S., Pintado, S., Escudero, E. C. & Galán-Mascarós, J. R. Fast and persistent electrocatalytic water oxidation by Co-Fe Prussian blue coordination polymers. *J. Am. Chem. Soc.* **135,** 13270–13273 (2013).

54. Goberna-Ferrón, S., Hernández, W. Y., Rodríguez-García, B. and Galán-Mascarós, J. R. Light-Driven Water Oxidation with Metal Hexacyanometallate Heterogeneous Catalysts. *ACS Catal.* **4,** 1637–1641 (2014).

55. Bui, H., Ahn, D. and Shrestha, N. Self-assembly of cobalt hexacyanoferrate crystals in 1-D array using ion exchange transformation route for enhanced electrocatalytic oxidation of alkaline and neutral water. *J. Mater. Chem. A* **4,** 9781–9788 (2016).

56. Ressnig, D., Shalom, M., Patscheider, J., More, R., Evangelisti, F., Antonietti, M. and Patzke, G. Photochemical and electrocatalytic water oxidation activity of cobalt carbodiimide. *J. Mater. Chem. A* **3,** 5072–5082 (2015).

57. Patscheider, J., Ressnig, D., Shalom, M., More, R., Evangelisti, F., Antonietti, M. and Patzke, G. Photochemical and electrocatalytic water oxidation activity of cobalt carbodiimide. *J. Mater. Chem. A* **3,** 5072–5082 (2015).

58. Dolomanov, O. V, Blake, A. J., Champness, N. R. and Schröder, M. {\it OLEX}: new software for visualization and analysis of extended crystal structures. *J. Appl. Crystallogr.* **36,** 1283–1284 (2003).

59. Tekin, A., Karalti, O. and Karadas, F. A metal dicyanamide cluster with high CO_2/N_2 selectivity. *Microporous Mesoporous Mater.* **228,** 153–157 (2016).

60. Mason, J. A., Sumida, K., Herm, Z. R., Krishna, R. and Long, J. R. Evaluating metal–organic frameworks for post-combustion carbon dioxide capture via temperature swing adsorption. *Energy Environ. Sci.* **4,** 3030–3040 (2011).

61. Li, J. R., Ma, Y., McCarthy, M. C., Sculley, J., Yu, J., Jeong, H. K., Balbuena, P. B. and Zhou, H.C. Carbon dioxide capture-related gas adsorption and separation in metal-organic frameworks. *Coord. Chem. Rev.* **255,** 1791–1823 (2011).

62. Sumida, K., Rogow, D.L., Mason, J. A., McDonald, T. M., Bloch, E. D., Hern, Z.R., Bae, T. H. and Long, J.R. Carbon dioxide capture in metal-organic frameworks. *Chem. Rev.* **112,** 724–781 (2012).

63. Batten, S., Jensen, P. and Kepert, C. Syntheses, structures and magnetism of α-$Mn(dca)_2$, $[Mn(dca)_2(H_2O)_2]\cdot H_2O$, $[Mn(dca)_2(C_2H_5OH)_2]\cdot(CH_3)_2CO$, $[Fe(dca)_2(CH_3OH)_2]$ and $[Mn(dca)_2(L)_2]$, where L = pyridine, CH_3OH or DMF and dca= dicyanamide, N(CN)2. *J. Chem. Soc., Dalt. Trans.* **22,** 2987–2997 (1999).

64. McIntyre, N. S. and Cook, M. G. X-ray photoelectron studies on some oxides and hydroxides of cobalt, nickel, and copper. *Anal. Chem.* **47,** 2208–2213 (1975).

65. Biesinger, M. C., Payne, B. P., Grosvenor, A.P., Lau, L.W., Gerson, A. R. and Smart, R. Resolving surface chemical states in XPS analysis of first row transition metals, oxides and hydroxides: Cr, Mn, Fe, Co and Ni. *Appl. Surf. Sci.* **257,** 2717–2730 (2011).

66. Aksoy, M., Nune, S. V. K. and Karadas, F. A Novel Synthetic Route for the

Preparation of an Amorphous Co/Fe Prussian Blue Coordination Compound with High Electrocatalytic Water Oxidation Activity. *Inorg. Chem.*, **55**, 4301-4307(2016)

67. Petitto, S. C., Marsh, E. M. and Carson, G. A. Cobalt oxide surface chemistry: The interaction of CoO(100), Co_3O_4(110) and Co_3O_4(111) with oxygen and water. *J. Mol. Catal. A Chem.* **281,** 49–58 (2008).

68. Wasylenko, D. J., Ganesamoorthy, C., Borau-Garcia, J. and Berlinguette, C. P. Electrochemical evidence for catalytic water oxidation mediated by a high-valent cobalt complex. *Chem. Commun.* **47,** 4249–4251 (2011).

69. Surendranath, Y., Kanan, M. W. and Nocera, D. G. Mechanistic Studies of the Oxygen Evolution Reaction by a Cobalt-Phosphate Catalyst at Neutral pH. *J. Am. Chem. Soc.* **132,** 16501–16509 (2010).

70. Zou, X., Su, J., Silva, R., Goswami, A., Sathe, B. R. and Asefa, T. Efficient oxygen evolution reaction catalyzed by low-density Ni-doped Co_3O_4 nanomaterials derived from metal-embedded graphitic C_3N_4. *Chem. Commun. (Camb).* **49,** 7522–7524 (2013).

71. Wu, J., Liao, L. and Yan, W. Polyoxometalates immobilized in ordered mesoporous carbon nitride as highly efficient water oxidation catalysts. *ChemSusChem* **5,** 1207–1212 (2012).